ARTICLE

https://doi.org/10.1038/s41586-019-1064-z

Genetic compensation triggered by mutant mRNA degradation

Mohamed A. El-Brolosy[1], Zacharias Kontarakis[1,8], Andrea Rossi[1,4,8], Carsten Kuenne[2], Stefan Günther[2], Nana Fukuda[1], Khrievono Kikhi[1], Giulia L. M. Boezio[1], Carter M. Takacs[3,5], Shih-Lei Lai[1,6], Ryuichi Fukuda[1], Claudia Gerri[1,7], Antonio J. Giraldez[3] & Didier Y. R. Stainier[1]*

Genetic robustness, or the ability of an organism to maintain fitness in the presence of harmful mutations, can be achieved via protein feedback loops. Previous work has suggested that organisms may also respond to mutations by transcriptional adaptation, a process by which related gene(s) are upregulated independently of protein feedback loops. However, the prevalence of transcriptional adaptation and its underlying molecular mechanisms are unknown. Here, by analysing several models of transcriptional adaptation in zebrafish and mouse, we uncover a requirement for mutant mRNA degradation. Alleles that fail to transcribe the mutated gene do not exhibit transcriptional adaptation, and these alleles give rise to more severe phenotypes than alleles displaying mutant mRNA decay. Transcriptome analysis in alleles displaying mutant mRNA decay reveals the upregulation of a substantial proportion of the genes that exhibit sequence similarity with the mutated gene's mRNA, suggesting a sequence-dependent mechanism. These findings have implications for our understanding of disease-causing mutations, and will help in the design of mutant alleles with minimal transcriptional adaptation-derived compensation.

Recent advances in reverse genetics tools have greatly enhanced our ability to analyse gene function in a wide range of organisms. These studies have reinforced previous observations that many engineered mutants do not exhibit an obvious phenotype, reviving interest in the concept of genetic robustness. Several mechanisms have been proposed to explain genetic robustness, including functional redundancy[1], rewiring of genetic networks[2] and, in the case of rapidly proliferating organisms such as yeast, the acquisition of adaptive mutations[3]. In a previous report[4], we proposed genetic compensation—and specifically, transcriptional adaptation[5]—as another underlying mechanism. According to this model, a mutation can lead to the increased expression of related genes that are themselves able to assume the function of the mutated gene. We provided evidence that this increased expression could be induced by a process upstream of the loss of protein function, indicating the existence of an unknown trigger. Here, to investigate the underlying molecular machinery, we developed and investigated several models of transcriptional adaptation in zebrafish and mouse.

Transcriptional adaptation in zebrafish and mouse

We began by analysing different zebrafish and mouse mutants that either have a premature termination codon (PTC) or have their last exon deleted (Extended Data Fig. 1). In zebrafish, *hbegfa*, *vcla*, *hif1ab*, *vegfaa*, *egfl7* and *alcama* mutants exhibit increased mRNA expression levels of a gene paralogue or family member (hereafter referred to as 'adapting gene'), namely, *hbegfb*, *vclb*, *epas1a* and *epas1b*, *vegfab*, *emilin3a* and *alcamb*, respectively (Fig. 1a). Injection of wild-type *hif1ab*, *vegfaa*, *egfl7* and *alcama* mRNA into the respective mutants did not have any effect on this transcriptional adaptation response (Extended Data Fig. 2a), suggesting that it is triggered upstream of the loss of protein function. Moreover, we found that *vcla*, *hif1ab* and *egfl7* heterozygous animals also displayed transcriptional adaptation, albeit less pronounced than that observed in the homozygous mutants (Extended Data Fig. 2b), indicating that transcriptional adaptation is a dominant phenomenon. Notably, we also observed an upregulation of the wild-type allele in *hbegfa*, *hif1ab*, *vegfaa* and *alcama* heterozygous embryos (Extended Data Fig. 2c). Similarly, we found that *Fermt2* (also known as *Kindlin-2*) mutant mouse kidney fibroblasts (MKFs), *Rela* and *Actg1* mutant mouse embryonic fibroblasts (MEFs) and *Actb* mutant mouse embryonic stem cells (mESCs) (hereafter referred to as the knockout alleles) displayed increased mRNA levels of *Fermt1* (also known as *Kindlin-1*), *Rel*, *Actg2* and *Actg1*, respectively (Fig. 1b). Transfection of wild-type *Fermt2* and *Rela* in the respective knockout cells did not dampen the transcriptional adaptation response (Extended Data Fig. 2d–f), and we also found that *Actb* heterozygous mESCs upregulated *Actg1* (Extended Data Fig. 2g). Altogether, these data strongly indicate that the loss of protein function is not the trigger for the transcriptional adaptation response observed in these models.

To determine whether the increased mRNA expression levels were caused by increased transcription of the adapting gene or increased mRNA stability, we measured the precursor mRNA (pre-mRNA) levels of *hbegfb* and *emilin3a* in *hbegfa* and *egfl7* zebrafish mutants, and found that they were also upregulated (Extended Data Fig. 3a). Similar findings were obtained for *Fermt1* and *Rel* pre-mRNA expression levels in *Fermt2* and *Rela* knockout mouse cells (Extended Data Fig. 3b). Together, these data indicate an increase in transcription of the adapting genes. In addition, *Fermt2* knockout MKFs displayed increased chromatin accessibility at the *Fermt1* transcription start site (TSS), as observed by the assay for transposase-accessible chromatin with high-throughput sequencing (ATAC-seq) (Extended Data Fig. 3c).

RNA decay triggers transcriptional adaptation

As the loss of protein function does not appear to be the trigger for the transcriptional adaptation response, we investigated two other possibilities: the DNA lesion and the mutant mRNA. In the context of the

[1]Department of Developmental Genetics, Max Planck Institute for Heart and Lung Research, Bad Nauheim, Germany. [2]ECCPS Bioinformatics and Deep Sequencing Platform, Max Planck Institute for Heart and Lung Research, Bad Nauheim, Germany. [3]Department of Genetics, Yale University School of Medicine, New Haven, CT, USA. [4]Present address: Leibniz Research Institute for Environmental Medicine, Düsseldorf, Germany. [5]Present address: University of New Haven, New Haven, CT, USA. [6]Present address: Institute of Biomedical Sciences, Academia Sinica, Taipei, Taiwan. [7]Present address: The Francis Crick Institute, London, UK. [8]These authors contributed equally: Zacharias Kontarakis, Andrea Rossi. *e-mail: didier.stainier@mpi-bn.mpg.de

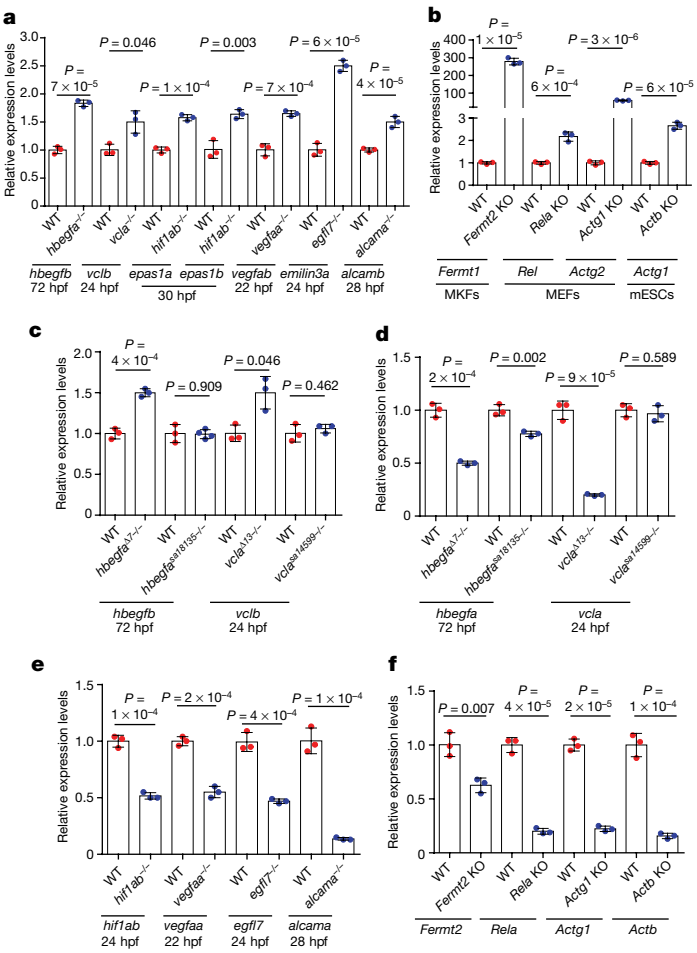

Fig. 1 | Transcriptional adaptation in zebrafish and mouse correlates with mutant mRNA decay. a, Quantitative polymerase chain reaction (qPCR) analysis of *hbegfb*, *vclb*, *epas1a*, *epas1b*, *vegfab*, *emilin3a* and *alcamb* mRNA expression levels in *hbegfa*, *vcla*, *hif1ab*, *vegfaa*, *egfl7* and *alcama* wild-type (WT) and homozygous mutant (−/−) zebrafish. hpf, hours post-fertilization. **b**, qPCR analysis of *Fermt1*, *Rel*, *Actg2* and *Actg1* mRNA expression levels in *Fermt2*, *Rela*, *Actg1* and *Actb* wild-type and knockout (KO) cells. **c**, **d**, qPCR analysis of *hbegfb* and *vclb* (**c**) and *hbegfa* and *vcla* (**d**) mRNA expression levels in the indicated *hbegfa* and *vcla* mutant alleles. **e**, qPCR analysis of *hif1ab*, *vegfaa*, *egfl7* and *alcama* mRNA expression levels in *hif1ab*, *vegfaa*, *egfl7* and *alcama* wild-type and mutant zebrafish. **f**, qPCR analysis of *Fermt2*, *Rela*, *Actg1* and *Actb* mRNA expression levels in *Fermt2*, *Rela*, *Actg1* and *Actb* wild-type and knockout cells. $n = 3$ biologically independent samples. Wild-type expression levels were set at 1. Data are mean ± s.d., and a two-tailed Student's *t*-test was used to calculate *P* values.

zebrafish studies, we identified several mutant alleles that did not display transcriptional adaptation (Extended Data Fig. 3d–f), indicating that a DNA lesion by itself is not sufficient to trigger transcriptional adaptation, or that specific DNA lesions are required. Notably, while analysing various mutant alleles, we found that unlike *hbegfa*$^{\Delta 7}$ and *vcla*$^{\Delta 13}$, two other PTC-bearing alleles, *hbegfa*^{sa18135} and *vcla*^{sa14599}, did not display transcriptional adaptation (Fig. 1c, Extended Data Fig. 1). To investigate the reason for this difference, we examined mutant mRNA levels and observed limited or no decrease in mRNA expression levels for the *hbegfa*^{sa18135} and *vcla*^{sa14599} alleles compared to wild type (Fig. 1d). This correlation between a decrease in mutant mRNA levels and transcriptional adaptation was observed for all alleles examined (Fig. 1e, f, Extended Data Fig. 3d–f). To determine whether the decreased mRNA levels were caused by decreased transcription or by reduced stability, we analysed pre-mRNA expression levels of *hbegfa*, *egfl7* and *alcama* in *hbegfa*$^{\Delta 7}$, *egfl7* and *alcama* mutants. We found that pre-mRNA expression levels remained unchanged or were slightly upregulated compared to wild type, in contrast with the mRNA levels (Extended Data Fig. 4a). Similar findings were observed in *Fermt2* and *Rela* knockout mouse cells (Extended Data Fig. 4b). Moreover, metabolic labelling of newly synthesized transcripts revealed similar or increased levels of *Fermt2*, *Rela* and *Actg1* mutant transcripts compared to wild type (Extended Data Fig. 4c), while transcription inhibition assays showed that the mutant transcripts had shorter half-lives (Extended Data Fig. 4d–f). Together, these data indicate that mutants that exhibit transcriptional adaptation have reduced mutant mRNA levels because of mRNA decay.

To investigate the role of the mRNA surveillance machinery in transcriptional adaptation, we genetically inactivated the key nonsense-mediated decay (NMD) factor Upf1[6] in *hbegfa*$^{\Delta 7}$, *vegfaa* and *vcla*$^{\Delta 13}$ zebrafish mutants. Inactivating *upf1* in these mutants led to a reduction in mutant mRNA decay (Extended Data Fig. 5a), and loss of transcriptional adaptation (Fig. 2a). We also observed a decrease in, or loss of, transcriptional adaptation in *Rela* and *Actb* knockout mouse cells when we knocked down proteins involved in the mRNA surveillance machinery (Fig. 2b, c, Extended Data Fig. 5b, c). Pharmacological inhibition of NMD in *hbegfa*$^{\Delta 7}$ zebrafish mutants (Extended Data Fig. 5d, e), and blocking translation in *Rela* knockout mouse cells (an alternative approach to inhibit mRNA decay) (Extended Data Fig. 5f, g) led to similar observations. We next investigated whether inducing mRNA degradation in wild-type zebrafish or in mouse cells by using uncapped RNAs, which are known to be rapidly degraded by 5′-to-3′ exonucleases[7], could trigger transcriptional adaptation. Indeed, injection of uncapped *hif1ab* or *vegfaa* RNAs into wild-type embryos induced transcriptional adaptation (Fig. 2d), including an increase in endogenous *hif1ab* and *vegfaa* expression (Extended Data Fig. 5h). Similarly, transfection of uncapped *Actb* RNA into wild-type mESCs led to *Actg1* upregulation (Extended Data Fig. 5i). Moreover, injecting wild-type embryos with uncapped *hif1ab* or *vegfaa* RNAs containing an upstream sequence that renders them resistant to 5′-to-3′ exonuclease-mediated decay[8] did not induce transcriptional adaptation (Extended Data Fig. 5j). Altogether, these data indicate that mRNA degradation is a major factor in triggering transcriptional adaptation. Notably, injection of uncapped RNA that was synthesized from the non-coding strand of *hif1ab* or *vegfaa* did not lead to an increase in *epas1a* or *vegfab* mRNA expression levels (Extended Data Fig. 5k), suggesting that the RNA sequence itself may have a role in transcriptional adaptation.

If mutant mRNA degradation is required for transcriptional adaptation, alleles that fail to transcribe the mutated gene should not display this response. To this end, we used CRISPR–Cas9 to generate such alleles (hereafter referred to as RNA-less alleles) by deleting promoter regions or the entire gene locus. RNA-less alleles of *hbegfa*, *vegfaa* and *alcama* failed to upregulate *hbegfb*, *vegfab* and *alcamb*, respectively (Fig. 3a). Similarly, in mouse cells, RNA-less alleles of *Rela*, *Actg1* and *Actb* did not upregulate the adapting gene (Fig. 3b). We also attempted to generate a promoter-less allele of *Fermt2* in MKFs; however, the obtained clones exhibited proliferation defects that prevented their expansion. As an alternative, we used CRISPR interference (CRISPRi) and found that reducing transcription of the mutant *Fermt2* gene in *Fermt2* knockout cells led to a decrease in *Fermt1* mRNA expression levels (Extended Data Fig. 6a). Notably, we observed that the promoter-less *Rela* MEFs were more sensitive to TNF-induced apoptosis[9] than the *Rela* knockout MEFs (Fig. 3c). Similarly, mESCs with a full locus deletion of *Actb* displayed less protrusive activity than *Actb* knockout cells (Fig. 3d, e). We also generated an *egfl7* RNA-less allele in zebrafish and observed that these mutants displayed pronounced vascular defects (Fig. 3f, g), and milder upregulation of the *emilin* genes (Extended Data Fig. 6b) compared to the phenotypically wild-type *egfl7*$^{\Delta 4}$ allele[4]. Furthermore, *vegfaa* promoter-less mutants displayed a stronger central artery sprouting phenotype than *vegfaa*$^{\Delta 10}$ mutants (Extended Data Fig. 6c); *hbegfa* RNA-less mutants displayed slow blood circulation—a phenotype not observed in *hbegfa*$^{\Delta 7}$ mutants (Extended

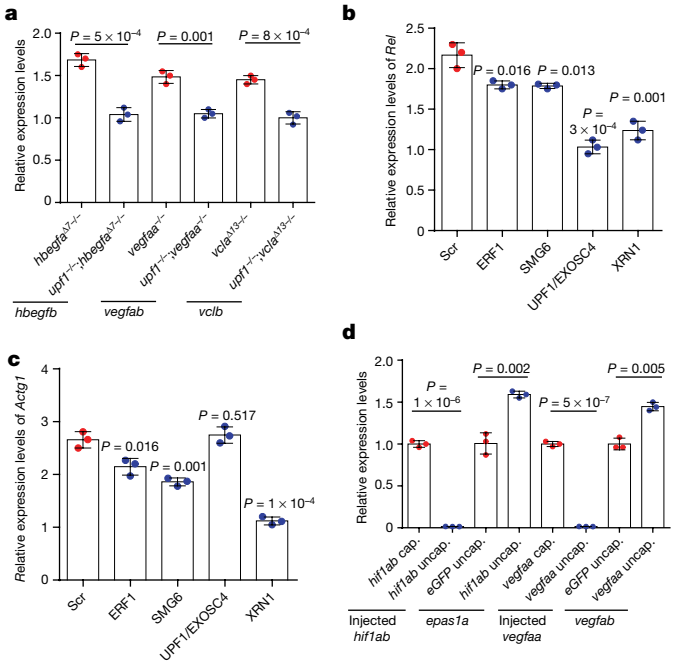

Fig. 2 | Mutant mRNA decay is required for transcriptional adaptation. **a**, qPCR analysis of *hbegfb*, *vegfab* and *vclb* mRNA expression levels in *upf1;hbegfa*, *upf1;vegfaa* and *upf1;vcla* double mutant zebrafish. **b**, qPCR analysis of *Rel* mRNA expression levels after siRNA-mediated knockdown of indicated proteins in *Rela* knockout mouse cells. Scr, scrambled siRNA control. **c**, qPCR analysis of *Actg1* mRNA expression levels after siRNA-mediated knockdown of indicated proteins in *Actb* knockout mouse cells. **d**, qPCR analysis of injected *hif1ab*, *epas1a*, injected *vegfaa* and *vegfab* mRNA expression levels in 6 hpf wild-type zebrafish embryos injected with the indicated RNA. cap, capped; uncap., uncapped. Wild-type or control expression levels were set at 1. $n = 3$ biologically independent samples. Data are mean ± s.d., and a two-tailed Student's *t*-test was used to calculate *P* values.

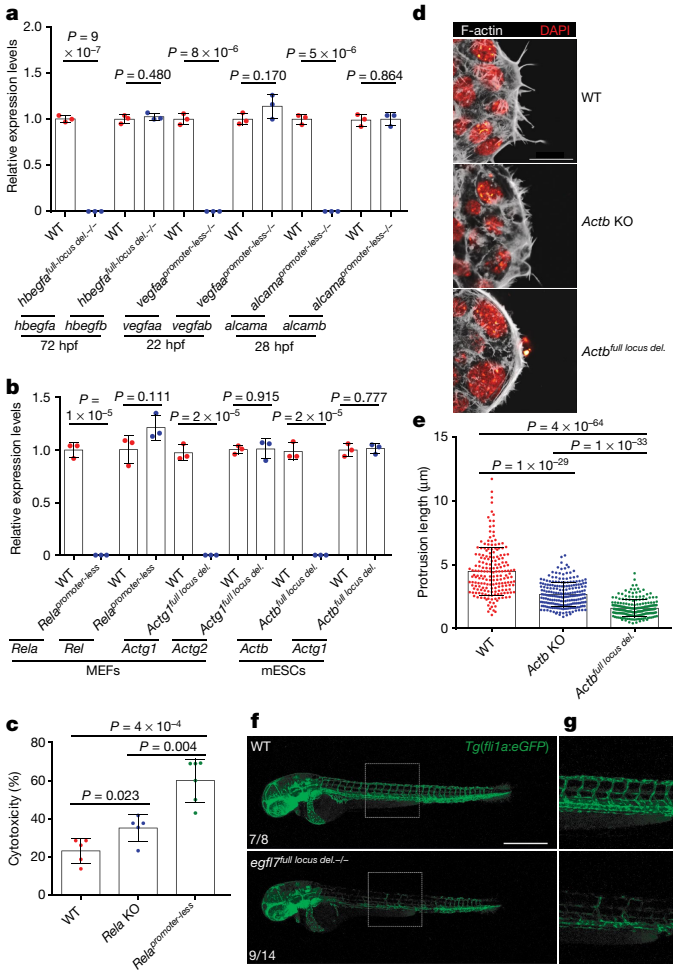

Fig. 3 | Alleles that fail to transcribe the mutated gene do not display transcriptional adaptation. **a**, qPCR analysis of *hbegfa*, *hbegfb*, *vegfaa*, *vegfab*, *alcama* and *alcamb* mRNA expression levels in zebrafish that lack the full *hbegfa* locus (full locus deletion; full locus del.) or the *vegfaa* or *alcama* promoter (promoter-less), compared to wild type. **b**, qPCR analysis of *Rela*, *Rel*, *Actg1*, *Actg2*, *Actb* and *Actg1* mRNA expression levels in MEFs and mESCs that lack the *Rela* promoter or the full *Actg1* or *Actb* locus, compared to wild-type cells. **c**, Cytotoxicity assay following TNF treatment of wild-type, *Rela* knockout and *Rela* promoter-less MEFs. Percentages are normalized relative to dimethyl sulfoxide (DMSO)-treated cells. **d**, Confocal microscopy of wild-type, *Actb* knockout and *Actb* full locus deletion mESCs. Actin filaments are depicted in white and nuclei in red (4′,6-diamidino-2-phenylindole (DAPI)). **e**, Actin filament protrusion length in wild-type, *Actb* knockout and *Actb* full locus deletion mESCs. **f**, Confocal micrographs of 48 hpf *Tg*(*fli1a*:eGFP) wild-type and *egfl7* full locus deletion mutant zebrafish. Lateral views; anterior is to the left. Higher magnifications of the dashed boxes are shown in **g**. Scale bars, 20 μm (**d**); 500 μm (**f**). Wild-type expression levels were set at 1 (**a**, **b**). $n = 3$ (**a**, **b**); $n = 5$ (**c**); and $n = 189$ (wild type), 219 (*Actb* knockout) and 205 (*Actb* full locus deletion) (**e**) independent samples. Data are mean ± s.d., and a two-tailed Student's *t*-test was used to calculate *P* values. The experiments in **d** and **f** were repeated twice independently with similar results.

data Fig. 6d); and *alcama* promoter-less mutants, but not *alcama*$^{\Delta 8}$ mutants, exhibited an elongated cardiac ventricle (Extended Data Fig. 6e). Therefore, use of RNA-less alleles can uncover phenotypes that are not observed in alleles exhibiting mutant mRNA degradation.

Sequence similarity and transcriptional adaptation

Next, we performed transcriptome analysis of *Fermt2*, *Actg1* and *Actb* knockout cells and observed that hundreds of genes were upregulated in the knockout cells compared to wild-type cells (Extended Data Fig. 7a). Only 81 genes were upregulated in all three of the knockout models, with no signs of a stress-induced response (Extended Data Fig. 7b, c, Supplementary Table 1). A first-pass analysis of the upregulated genes in each model showed that a disproportionate number of them exhibited sequence similarity with the mutated gene. We thus explored the relation between upregulation and sequence similarity based on several similarity thresholds (Extended Data Fig. 7d; see the 'Sequence similarity and subsampling analyses' section of the Methods) and found a significant correlation. Using the optimal 'expect' (*E*) values to identify similar genes, we observed that at least 50% of them were significantly upregulated in the different knockout cell models, compared to a maximum of 21% of non-similar genes (Fig. 4a, Extended Data Fig. 8a–c). Notably, seven of the twelve upregulated similar genes in *Actg1* knockout cells were not upregulated in *Actg1* RNA-less cells, and four of the six upregulated similar genes in *Actb* knockout cells were not upregulated in *Actb* RNA-less cells (Extended Data Fig. 8b, c). We also observed that four of the nine similar genes that were not upregulated in *Actg1* knockout cells at the mRNA level were upregulated at the pre-mRNA level (Extended Data Fig. 8d). Additional studies showed that injection of uncapped mouse *Actb* RNA into zebrafish embryos led to an increase in zebrafish *actb1* mRNA expression levels (Extended Data Fig. 8e, Supplementary Data), in line with the sequence similarity analyses mentioned above.

To begin to investigate how sequence similarity could have a role in transcriptional adaptation, we first injected uncapped transcripts containing only similar or non-similar sequences into zebrafish embryos. Using the *hif1ab* model, we observed that only transcripts containing sequences similar to *epas1a* led to an increase in *epas1a* mRNA expression levels (Fig. 4b, Extended Data Fig. 8f, Supplementary

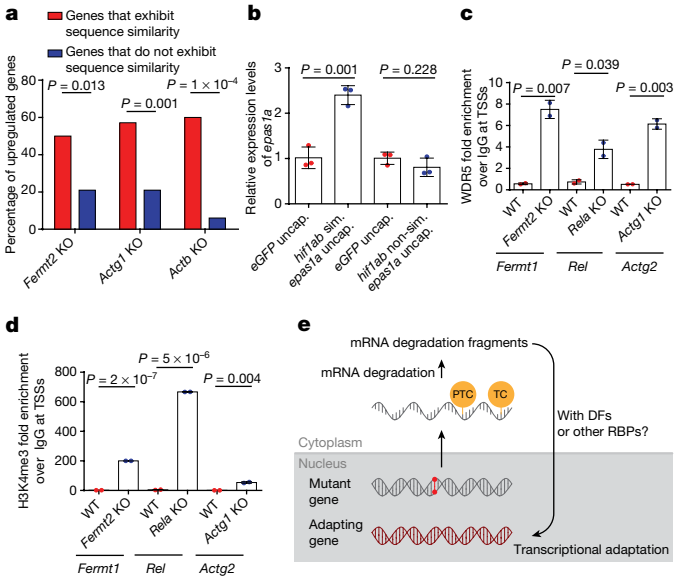

Fig. 4 | Transcriptional adaptation favours genes that exhibit sequence similarity with the mutated gene's mRNA, and is associated with permissive histone marks. a, Percentage of significantly upregulated (that is, where $\log_2$(gene expression level in knockout cells/gene expression level in wild-type cells) is greater than 0 and $P < 0.05$) protein-coding genes that exhibit sequence similarity (red) or do not exhibit sequence similarity (blue) with *Fermt2*, *Actg1* or *Actb*. **b**, qPCR analysis of *epas1a* mRNA expression levels in 6 hpf wild-type zebrafish that were injected with uncapped RNA composed solely of either the *hif1ab* mRNA sequences that are similar (sim.) to *epas1a* or the *hif1ab* mRNA sequences that are not similar (non-sim.) to *epas1a*. Control expression levels were set at 1. **c**, **d**, ChIP–qPCR analysis of WDR5 (**c**) and H3K4me3 (**d**) occupancy near the TSSs of *Fermt1*, *Rel* and *Actg2* in *Fermt2*, *Rela* and *Actg1* knockout mouse cells, respectively, compared to wild-type cells. Quantification of enrichment is shown as fold enrichment over IgG control. **e**, Current putative simplified model of transcriptional adaptation to mutations. DFs, decay factors; RBPs, RNA-binding proteins; TC, termination codon. $n = 3$ (**b**) or $n = 2$ (**c**, **d**) biologically independent samples. Data are mean ± s.d., and a two-tailed Student's *t*-test was used to calculate *P* values.

Data). We also generated synthetic transcripts that contained *hif1ab* sequences similar to the promoter, exons, introns or 3′ untranslated region (UTR) of *epas1a*. Injection of uncapped versions of these transcripts revealed that those exhibiting sequence similarity with exons or introns induced transcriptional adaptation, whereas those exhibiting sequence similarity with the 3′UTR did not; and the transcripts exhibiting sequence similarity with the promoter induced only a mild response (Extended Data Fig. 8g). These data are consistent with the transcriptome analyses of *Fermt2*, *Actg1* and *Actb* knockout cells (Extended Data Fig. 8a-c)—genes that exhibited sequence similarity with the mutated gene's mRNA in their 3′UTR were not upregulated, and genes that exhibited sequence similarity with promoters displayed a mild upregulation or were not upregulated. Altogether, these data suggest that, at least in some cases, sequence similarity has a role in transcriptional adaptation.

Epigenetic remodelling in adapting genes

In the past decade, it has become evident that the control of mRNA stability has an important role in gene expression[10–13]. Several studies have reported that mRNA decay factors can translocate to the nucleus and interact with histone modifiers and chromatin remodellers to modulate gene expression[14–17]. We thus performed a targeted small interfering RNA (siRNA) screen in *Rela* knockout cells to identify epigenetic modulators that are involved in transcriptional adaptation (Supplementary Table 2). Knockdown of the histone lysine demethylases KDM4 or KDM6, which remove the inhibitory H3K9me3 or H3K27me3 histone marks, respectively, dampened the transcriptional adaptation response; however, the strongest effect was observed after WDR5 knockdown (Extended Data Fig. 9a). WDR5 is part of the COMPASS complex, which generates the permissive histone mark H3K4me3. Chromatin immunoprecipitation (ChIP) revealed enrichment of WDR5 and H3K4me3 at the TSS of *Fermt1*, *Rel* and *Actg2* in *Fermt2*, *Rela* and *Actg1* knockout cells (Fig. 4c, d and Extended Data Fig. 9b). Moreover, knockdown of UPF1/EXOSC4 or XRN1 in *Rela* knockout cells led to the depletion of H3K4me3 at the *Rel* TSS (Extended Data Fig. 9c). Altogether, these data suggest a model in which concomitant with mutant mRNA degradation, decay factors translocate to the nucleus, where they bind to specific loci (possibly guided by decay intermediates) and recruit histone modifiers and/or chromatin remodellers to upregulate transcription (Fig. 4e and Extended Data Fig. 9d).

While investigating this model, we noted a study reporting that, in mESCs, transfection of short fragments of *Cdk9* or *Sox9* mRNA could lead to an increase in expression of these genes[18]. Mechanistically, these RNA fragments were found to downregulate native antisense transcripts that normally function as negative regulators of *Cdk9* and *Sox9* expression. Notably, we found that transfection of uncapped *Cdk9* or *Sox9* RNA also led to upregulation of these genes (Extended Data Fig. 10a). Furthermore, in another study[19], knockdown of a *BDNF* antisense transcript in HEK293T cells was reported to cause the upregulation of the sense transcript—a response that involved a decrease in the inhibitory H3K27me3 histone mark. We transfected HEK293T cells with uncapped *BDNF* sense RNA and observed a downregulation of the antisense transcript and a concomitant upregulation of the sense one (Extended Data Fig. 10b). Notably, we also observed a downregulation of antisense transcripts at the *hbegfb* and *vclb* loci in *hbegfa*$^{\Delta 7}$ and *vcla*$^{\Delta 13}$ mutants, respectively (Extended Data Fig. 10c, d). These data indicate that acting on antisense transcripts is another possible mechanism through which mRNA decay intermediates could induce transcriptional adaptation in a sequence-specific manner (Fig. 4e and Extended Data Fig. 9d).

Discussion

Despite its potential importance[5], transcriptional adaptation to mutations and its underlying molecular mechanisms remain poorly understood. Here we show that the mRNA surveillance machinery is important not only to prevent the translation of defective transcripts, but also to buffer against mutations by triggering the transcriptional upregulation of related genes, including the mutated gene itself (see Supplementary Discussion).

For several human genetic diseases, missense mutations or in-frame insertions or deletions (indels)—which are less likely to lead to mutant mRNA degradation—are reportedly more common than potentially mRNA-destabilizing nonsense mutations or out-of-frame indels[20–25]. Of note, a study on patients with Marfan syndrome reported that when compared to individuals with *FBN1* missense mutations, the mildest form of the disease was observed in an individual displaying very low mutant *FBN1* transcript levels owing to an out-of-frame indel that led to a PTC in the *FBN1* coding sequence[26]. Similar observations have been described for mutations in the *HBB* gene[27]. The current dogma is that pathogenic missense mutations tend to be more common in affected individuals because they might lead to constitutively active or dominant negative proteins. However, we propose that nonsense mutations are less common as they might result in mRNA decay-triggered upregulation of related genes and therefore not cause noticeable symptoms. Detailed transcriptomic analyses of relevant individuals will help to test this hypothesis. Moreover, studies[28,29] of healthy individuals have reported homozygous loss-of-function mutations in several genes (including *EGFL7* and *RELA*, the zebrafish and mouse homologues of which we studied here), and it will be interesting to investigate whether degradation of the mutant transcripts is associated with a transcriptional adaptation response that protects them. Such analyses may help us to understand why some mutations cause disease whereas others do not. They may also help in the identification of modifier genes, the expression levels of which could be further modulated for therapeutic purposes.

Online content

Any methods, additional references, Nature Research reporting summaries, source data, statements of data availability and associated accession codes are available at https://doi.org/10.1038/s41586-019-1064-z.

Received: 3 December 2017; Accepted: 5 February 2019;
Published online 3 April 2019.

1. Tautz, D. Redundancies, development and the flow of information. *BioEssays* **14**, 263–266 (1992).
2. Barabási, A. L. & Oltvai, Z. N. Network biology: understanding the cell's functional organization. *Nat. Rev. Genet.* **5**, 101–113 (2004).
3. Teng, X. et al. Genome-wide consequences of deleting any single gene. *Mol. Cell* **52**, 485–494 (2013).
4. Rossi, A. et al. Genetic compensation induced by deleterious mutations but not gene knockdowns. *Nature* **524**, 230–233 (2015).
5. El-Brolosy, M. A. & Stainier, D. Y. R. Genetic compensation: a phenomenon in search of mechanisms. *PLoS Genet.* **13**, e1006780 (2017).
6. Isken, O. & Maquat, L. E. Quality control of eukaryotic mRNA: safeguarding cells from abnormal mRNA function. *Genes Dev.* **21**, 1833–1856 (2007).
7. Mukherjee, C. et al. Identification of cytoplasmic capping targets reveals a role for cap homeostasis in translation and mRNA stability. *Cell Reports* **2**, 674–684 (2012).
8. Boehm, V., Gerbracht, J. V., Marx, M. C. & Gehring, N. H. Interrogating the degradation pathways of unstable mRNAs with XRN1-resistant sequences. *Nat. Commun.* **7**, 13691 (2016).
9. Doi, T. S. et al. Absence of tumor necrosis factor rescues RelA-deficient mice from embryonic lethality. *Proc. Natl Acad. Sci. USA* **96**, 2994–2999 (1999).
10. Hao, S. & Baltimore, D. The stability of mRNA influences the temporal order of the induction of genes encoding inflammatory molecules. *Nat. Immunol.* **10**, 281–288 (2009).
11. Elkon, R., Zlotorynski, E., Zeller, K. I. & Agami, R. Major role for mRNA stability in shaping the kinetics of gene induction. *BMC Genomics* **11**, 259 (2010).
12. Rabani, M. et al. Metabolic labeling of RNA uncovers principles of RNA production and degradation dynamics in mammalian cells. *Nat. Biotechnol.* **29**, 436–442 (2011).
13. Sun, M. et al. Comparative dynamic transcriptome analysis (cDTA) reveals mutual feedback between mRNA synthesis and degradation. *Genome Res.* **22**, 1350–1359 (2012).
14. Collins, S. R. et al. Functional dissection of protein complexes involved in yeast chromosome biology using a genetic interaction map. *Nature* **446**, 806–810 (2007).
15. Berretta, J., Pinskaya, M. & Morillon, A. A cryptic unstable transcript mediates transcriptional *trans*-silencing of the Ty1 retrotransposon in *S. cerevisiae*. *Genes Dev.* **22**, 615–626 (2008).
16. Pinskaya, M., Gourvennec, S. & Morillon, A. H3 lysine 4 di- and tri-methylation deposited by cryptic transcription attenuates promoter activation. *EMBO J.* **28**, 1697–1707 (2009).
17. Haimovich, G. et al. Gene expression is circular: factors for mRNA degradation also foster mRNA synthesis. *Cell* **153**, 1000–1011 (2013).
18. Ghanbarian, H. et al. Small RNA-directed epigenetic programming of embryonic stem cell cardiac differentiation. *Sci. Rep.* **7**, 41799 (2017).
19. Modarresi, F. et al. Inhibition of natural antisense transcripts *in vivo* results in gene-specific transcriptional upregulation. *Nat. Biotechnol.* **30**, 453–459 (2012).
20. Eisensmith, R. C. & Woo, S. L. Molecular basis of phenylketonuria and related hyperphenylalaninemias: mutations and polymorphisms in the human phenylalanine hydroxylase gene. *Hum. Mutat.* **1**, 13–23 (1992).
21. Myerowitz, R. Tay-Sachs disease-causing mutations and neutral polymorphisms in the Hex A gene. *Hum. Mutat.* **9**, 195–208 (1997).
22. Genschel, J. & Schmidt, H. H. Mutations in the LMNA gene encoding lamin A/C. *Hum. Mutat.* **16**, 451–459 (2000).
23. Chuzhanova, N. A., Anassis, E. J., Ball, E. V., Krawczak, M. & Cooper, D. N. Meta-analysis of indels causing human genetic disease: mechanisms of mutagenesis and the role of local DNA sequence complexity. *Hum. Mutat.* **21**, 28–44 (2003).
24. Ferec, C. & Cutting, G. R. Assessing the disease-liability of mutations in CFTR. *Cold Spring Harb. Perspect. Med.* **2**, a009480 (2012).
25. Zhou, Q. et al. Early-onset stroke and vasculopathy associated with mutations in ADA2. *N. Engl. J. Med.* **370**, 911–920 (2014).
26. Dietz, H. C. et al. Four novel FBN1 mutations: significance for mutant transcript level and EGF-like domain calcium binding in the pathogenesis of Marfan syndrome. *Genomics* **17**, 468–475 (1993).
27. Hall, G. W. & Thein, S. Nonsense codon mutations in the terminal exon of the β-globin gene are not associated with a reduction in β-mRNA accumulation: a mechanism for the phenotype of dominant β-thalassemia. *Blood* **83**, 2031–2037 (1994).
28. Sulem, P. et al. Identification of a large set of rare complete human knockouts. *Nat. Genet.* **47**, 448–452 (2015).
29. Lek, M. et al. Analysis of protein-coding genetic variation in 60,706 humans. *Nature* **536**, 285–291 (2016).

Acknowledgements We thank V. Serobyan, F. Mueller, Z. Jiang, A. Beisaw and F. Gunawan for discussion and comments on the manuscript; J. Pestel for the *alcama* mutant; A. Atzberger for support with cell sorting; and N. Gehring and V. Böhm for providing the XRN1-resistant sequence plasmid. M.A.E.-B. was supported by a Boehringer Ingelheim Fonds PhD fellowship. Research in the D.Y.R.S. laboratory is supported by the Max Planck Society, the EU, the DFG and the Leducq Foundation.

Reviewer information *Nature* thanks Miles Wilkinson and the other anonymous reviewer(s) for their contribution to the peer review of this work.

Author contributions M.A.E.-B. designed and performed most of the experiments, analysed the data and wrote the manuscript; Z.K. and A.R. designed and performed mESC experiments and some imaging and edited the manuscript; C.K. performed bioinformatics analyses; S.G. performed ATAC-seq and RNA-seq; N.F. generated some zebrafish mutants and performed some qPCR experiments; K.K. performed some qPCR experiments; G.L.M.B. performed some imaging; C.M.T. generated the *upf1* mutant, under the supervision of A.J.G.; S.-L.L., R.F. and C.G. provided unpublished mutants; and D.Y.R.S. helped to design the experiments and analyse data, supervised the work and wrote the manuscript. All authors commented on the manuscript.

Competing interests The authors declare no competing interests.

Additional information
Extended data is available for this paper at https://doi.org/10.1038/s41586-019-1064-z.
Supplementary information is available for this paper at https://doi.org/10.1038/s41586-019-1064-z.
Reprints and permissions information is available at http://www.nature.com/reprints.
Correspondence and requests for materials should be addressed to D.Y.R.S.
Publisher's note: Springer Nature remains neutral with regard to jurisdictional claims in published maps and institutional affiliations.

METHODS

Statistics and reproducibility. No statistical methods were used to predetermine sample size. The experiments were not randomized. The investigators were not blinded to allocation during experiments and outcome assessment. All experiments were performed at least twice unless otherwise noted. $P < 0.05$ was accepted as statistically significant.

Zebrafish husbandry. All zebrafish (*Danio rerio*, strain: Tüb/AB) husbandry was performed under standard conditions in accordance with institutional (Max Planck Gesellschaft) and national ethical and animal welfare guidelines approved by the ethics committee for animal experiments at the Regierungspräsidium Darmstadt, Germany (permit number B2/1017). All experiments were performed on zebrafish embryos or larvae between 6 hpf and 6 days post-fertilization (dpf). We used the following previously published mutant and transgenic lines: *hif1ab*^{bns90} (ref. [30]), *vegfaa*^{bns1} (ref. [31]), *egfl7*^{s980} (ref. [4]), *egfl7*^{s981} (ref. [4]), *hbegfa*^{sa18135} and *vcla*^{sa14599} (Sanger institute zebrafish mutation project; http://www.sanger.ac.uk/resources/zebrafish/zmp/), *Tg*(*fli1a:eGFP*)^{y1} (ref. [32]) and *TgBAC*(*etsrp:eGFP*)^{ci1} (ref. [33])

Cell culture. Wild-type and *Fermt2* knockout MKFs were a gift from R. Fässler. Wild-type and *Rela* knockout MEFs were a gift from A. Hoffmann. mESCs from the C57BL/6 mouse strain were a gift from J. Kim. None of the cell lines was authenticated by the authors. All cell lines tested negative for mycoplasma contamination.

Undifferentiated mESCs were maintained in PluriQ-ES-DMEM (MTI-GlobalStem), consisting of high-glucose DMEM supplemented with 15% ES cell-qualified fetal bovine serum (Millipore), 2 mM glutamine, 1% non-essential amino acids, 100 U ml^{-1} penicillin, 100 μg ml^{-1} streptomycin, 0.1 mM β-mercaptoethanol and 1,000 U ml^{-1} ESGRO (LIF, Chemicon international) and 2i (3 μM CHIR99021 and 1 μM PD0325901, Sigma). mESCs were grown in 0.1% gelatin-coated plates and passaged every second day. MEFs and MKFs were cultured in DMEM (Thermo) supplemented with 10% bovine calf serum (HyClone), 100 U ml^{-1} penicillin and 100 μg ml^{-1} streptomycin. All cells were grown at 37 °C, 95% humidity with 5% CO_2 and experiments were performed on cells passaged fewer than 20 times.

Genotyping. Heterozygous fish were incrossed; DNA and RNA were extracted from at least 24 individual embryos or larvae using TRIzol (Life Technologies) followed by phenol–chloroform extraction. In brief, single embryos or larvae were lysed and homogenized in TRIzol using a Next Advance Bullet Blender Homogenizer (Scientific Instrument Services). Chloroform was then added and phase separation was obtained following vortexing and centrifugation. The top aqueous phase (containing RNA) was isolated and stored at −80 °C and the bottom organic phase (containing DNA) was subjected to ethanol purification to precipitate the DNA. Purified DNA was then dissolved in water and genotyping was performed using high-resolution melt analysis or PCR. RNA from genotyped wild-type (+/+) and homozygous mutant (−/−)zebrafish was then pooled for further purification and cDNA synthesis. For each experiment, this process was performed on embryos from at least three different crosses.

High-resolution melt analysis was used to genotype all mutant zebrafish and mouse cell lines, with the exception of the RNA-less alleles, which were genotyped by PCR. The primer sequences used for genotyping are listed in Supplementary Table 3.

qPCR expression analysis. qPCR was performed in a CFX Connect Real-Time System (Biorad). RNA was isolated using TRIzol and at least 500 ng RNA was used for reverse transcription using the Maxima First Strand cDNA synthesis kit (Thermo). All reactions were performed in at least technical duplicates and the results represent biological triplicates. qPCR was performed at the embryonic or larval stage when the wild-type version of the mutated gene exhibits its highest level of expression. For *hbegfa* mutants treated with the NMD inhibitor, data were analysed at 6 dpf and not at 72 hpf, as the drug seemed to be effective only when used for three days between 72 hpf and 6 dpf; treatment of earlier-stage embryos was not possible owing to toxicity. Primers were designed using Primer3 (http://biotools.umassmed.edu/bioapps/primer3_www.cgi). Primers to detect pre-mRNA were designed to bind around intron–exon boundaries. Allele-specific primers were designed in such a way as to amplify the wild-type but not the mutant allele. To determine the injected capped and uncapped RNA levels, a universal reverse primer corresponding to the adaptor sequence at the 3′ end of the injected RNAs was used, along with forward primers designed in close proximity; in this way we were able to distinguish between endogenous and injected RNAs. Several primer pairs along the cDNA of the gene were used to assess transcription in the candidate promoter-less alleles. Only mutant alleles exhibiting less than 10% of wild-type mRNA levels with all the above mentioned primer pairs were used in the study. For the *upf1* double mutant data, the figures show expression levels of the adapting gene in the double mutants relative to its expression levels in the *upf1* single mutants. Expression levels of the mutated gene in the *upf1* double mutants are relative to those in *hbegfa*, *vegfaa* or *vcla* single mutants. Equal numbers of cells were used for the cell line qPCR experiments. *rpl13* and *gapdh*, and *Actb*, *Rn18s* and *Gapdh*, were used to normalize zebrafish and mouse experiments, respectively. *rpl13* was chosen as a reference gene for zebrafish experiments as its expression levels were not changed between wild-type and *egfl7*[4], *hbegfa*, *vcla*, *vegfaa* and *alcama* mutant embryos (unpublished microarray data). Primer sequences used for the qPCR experiments are listed in Supplementary Table 4. Fold changes were calculated using the $2^{-\Delta\Delta Ct}$ method. All C_t and ΔC_t values are listed in the Source Data files. C_t values for the reference genes ranged between 12 and 23 except for *Rn18s*, which ranged between 6 and 8.

In vitro transcription and RNA microinjections. cDNAs encoding *hif1ab*, *vegfaa*, *egfl7* and *alcama* full-length mRNAs were amplified using whole-embryo cDNA as a template. PCR fragments were ligated into a pCS2+ vector between BamHI and XbaI (NEB) sites. All constructs were verified by sequencing. Plasmids were linearized using NotI (NEB) and in vitro transcribed using the mMESSAGE mMACHINE SP6 kit (Life Technologies). RNA was then purified using an RNA Clean and Concentrator kit (Zymo Research). Approximately 10–100 pg of each mRNA was injected into embryos from heterozygous incrosses at the one-cell stage. At 22–30 hpf, embryos were collected in TRIzol for qPCR analysis.

To transcribe uncapped RNAs, cDNA was used to amplify zebrafish *hif1ab* and *vegfaa* and mouse *Actb*, whereas genomic DNA was used to amplify mouse *Cdk9* and *Sox9* (single exon for *Cdk9* and the entire genomic locus (exons and introns) for *Sox9*) as their expression levels were too low to amplify from cDNA. In all cases, a reverse primer containing the adaptor sequence 5′-GCCAAGCTATTTAGGTGACACTATAG-3′ was used for amplification. A reverse primer containing only the adaptor sequence was subsequently used for qPCR detection of the injected transcripts, as described above. To generate uncapped XRN1-resistant transcripts, the XRN1-resistant sequence[8] was cloned upstream of the *hif1ab* and *vegfaa* coding sequences in pCS2+, and then linearized using NotI for in vitro transcription. In vitro synthesis of uncapped transcripts was performed using SP6 (or T7 in the case of the uncapped RNAs corresponding to the non-coding strand) RNA polymerase (Promega) and the RNA was purified using an RNA Clean and Concentrator kit. Alternatively, a T7 sequence was added to the forward primer of the PCR reaction and the product was directly used for in vitro synthesis of uncapped RNAs. The RNAs were injected into one-cell-stage zebrafish embryos (50 pg) or transfected into cells (1 μg) in 12-well plates.

In vitro generation of synthetic transcripts containing different sequences of *hif1ab* mRNA. Oligonucleotides containing *hif1ab* sequences similar to *epas1a* were ligated together along with a 5′ T7 promoter sequence. Similar sequences were identified using a highly sensitive BLASTn analysis with a word size of 7 and an *E* value of up to 1,000,000. The alignment was visualized using Kablammo at the less sensitive *E* value of 25 owing to display constraints (Extended Data Fig. 8f). The same approach was used to generate transcripts of *hif1ab* sequences that were not similar to *epas1a*, using the non-alignable sequences. In vitro transcription was performed using the T7 RNA polymerase (Promega).

Guide RNA design. Guide RNAs (gRNAs) were designed using the CRISPR design tool CHOPCHOP (http://chopchop.cbu.uib.no/)[34]. To generate RNA-less alleles, double gRNAs were designed to flank the region to be deleted. gRNAs that were used to delete promoter regions were designed at least 500 bp upstream and downstream from the TSS of the respective gene. Sequences of the gRNAs used in this study and their genomic binding sites are listed in Supplementary Table 5.

Generation of zebrafish mutants. *alcama* mutant fish were generated using the TALEN technology[35,36]. The other mutants were generated using the CRISPR–Cas9 system as previously described[37,38]. To generate mutants, *Cas9* mRNA (100 pg) and a gRNA targeting the gene of interest (50 pg) were co-injected into zebrafish embryos at the one-cell stage. To generate RNA-less alleles, two gRNAs were co-injected with *Cas9* mRNA. The following mutants were generated for this study: *hbegfa*^{bns189} (*hbegfa*$^{\Delta 7}$), *hbegfa*^{bns203} (*hbegfa*$^{\Delta 3}$), *hbegfa*^{bns243} (*hbegfa*$^{full\ locus\ del.}$), *vcla*^{bns241} (*vcla*$^{\Delta 13}$), *vcla*^{bns300} (*vcla*$^{exon22\_ins1}$), *vegfaa*^{bns301} (*vegfaa*$^{5'UTR\Delta 10}$), *vegfaa*^{bns242} (*vegfaa*$^{promoter\text{-}less}$), *egfl7*^{bns303} (*egfl7*$^{5'UTR\Delta 3}$), *egfl7*^{bns302} (*egfl7*$^{full\ locus\ del.}$), *alcama*^{bns201} (*alcama*$^{\Delta 10}$), *alcama*^{bns244} (*alcama*$^{promoter\text{-}less}$) and *upf1*^{ya3319} (*upf1*$^{\Delta 3ins1}$).

hbegfa$^{\Delta 7}$, *hbegfa*^{sa18135}, *hbegfa*$^{full\ locus\ del.}$, *vcla*$^{\Delta 13}$, *vcla*^{sa14599}, *vcla*$^{exon22\_ins1}$, *alcama*$^{\Delta 10}$ and *alcama*$^{promoter\text{-}less}$ mutants do not exhibit any obvious defects under a dissecting microscope. *upf1* mutants exhibit pericardial oedema by 5 dpf and die by 10 dpf.

Transfections and isolation of mutant mouse cell clones. *Fermt2* knockout MKFs and *Rela* knockout MEFs were previously published[39,40]. The other mutants were generated using the CRISPR–Cas9 system. gRNAs targeting *Rela*, *Actg1* and *Actb* were cloned into the PX458 or PX459 vectors (Addgene; 48138 and 62988) as previously described[41]. The final bicistronic vector (hereafter referred to as nuclease plasmid) encoded the gRNA and the Cas9 nuclease. mESCs were transfected with nuclease plasmids in antibiotic-free medium in a 24-well plate using Xfect (Takara) according to the manufacturer's protocol, and transferred into a 10-cm dish the next day. Transfected cells were selected with 0.5 μg ml^{-1} puromycin (Sigma) for four days and clones were isolated and genotyped using high-resolution melt analysis and sequencing. MEFs were electroporated using Nucleofection (Lonza) with

5 μg nuclease plasmid DNA, according to the manufacturer's protocol. Two days after transfection, cells expressing eGFP were subjected to single-cell sorting into 96-well plates using a FACSAria III (BD Biosciences). Three to four weeks after single-cell sorting, clones were isolated and genotyped by PCR and sequencing. For generation of RNA-less alleles, cells were co-transfected with two nuclease plasmids.

Actg1^{NSD} (*Actg1* knockout) and *Actg1*$^{full\ locus\ del.}$ mutant MEFs do not exhibit any gross morphological defects.

Overexpression plasmids. *Fermt2* and *Rela* cDNAs were amplified using MEF cDNA as a template. PCR fragments were ligated into the pcDNA3.1 mammalian expression vector (Thermo) between the BamHI and XbaI sites. Plasmids were transfected into the respective knockout cells using FuGENE 6 (Promega) according to the manufacturer's protocol. Two days after transfection, cells were selected with 0.5 mg ml^{-1} and 2 mg ml^{-1} G418 (Sigma) for *Fermt2* and *Rela* knockout cells, respectively. A week later, cells were lysed in modified radioimmunoprecipitation assay (RIPA) buffer for western blot analysis.

Uncapped RNA transfections. Uncapped *eGFP*, *Actb*, *Cdk9* and *Sox9* RNAs were transfected into mESCs or MEFs using Lipofectamine Messenger Max (Thermo) transfection reagent according to the manufacturer's protocol. Six hours after transfection, cells were trypsinized and collected in TRIzol for RNA extraction.

CRISPR interference. Three gRNAs targeting the *Fermt2* promoter and TSS were each cloned into a plasmid encoding a fusion protein of catalytically dead Cas9 and Krüppel-associated box (KRAB) repressor (Addgene, 71237), as previously described[42]. *Fermt2* knockout cells were transfected with the three plasmids and 48 h after transfection, cells positive for eGFP were sorted into TRIzol for RNA extraction.

RNA interference. siRNAs are listed in Supplementary Table 2. siRNA transfections were performed using the RNAiMAX transfection reagent (Thermo) according to the manufacturer's protocol. Forty-eight hours after transfection, cells were collected in TRIzol for RNA extraction, except for knockdowns of SMG6, ERF1 and XRN1 (in which cases cells were collected 24 h after transfection). In most cases, siRNAs were used at 10 nM and gave a knockdown efficiency of 70–90% (as assessed by mRNA levels). However, to knock down XRN1 in mESCs, a lower concentration of siRNAs was used (2.5 nM, which led to a knockdown efficiency of 20%) as stronger knockdown affected housekeeping genes as well (data not shown). A scrambled siRNA (Sigma, SIC00), which does not bind to any of the mouse transcripts, was used as a negative control.

For each experiment, the figures show expression levels of the adapting gene in knockout cells relative to its expression levels in wild-type cells that were treated with the same siRNA. Expression levels of the mutant gene in the knockout cells treated with a given siRNA are relative to those in knockout cells treated with scrambled siRNA. All C_t and ΔC_t values are shown in the Source Data files.

Pharmacological treatments. To inhibit NMD, 72 hpf wild-type and *hbegfa* mutant larvae were treated with 10 μM NMDi14[43] or DMSO, and three days later, they were collected in TRIzol for qPCR analysis. No gross alterations were observed in the drug-treated larvae. To inhibit RNA degradation through translation blockade, wild-type and *Rela* knockout cells were treated with 200 μg ml^{-1} cycloheximide (Sigma) or DMSO for 5 h, then collected in TRIzol for RNA extraction.

For each experiment, the figures show expression levels of the adapting gene in mutant larvae or knockout cells, relative to its expression levels in wild-type larvae or cells that were treated with the same drug. Expression levels of the mutated gene in the mutant larvae, or knockout cells treated with a given drug, are relative to those in untreated mutant larvae, or knockout cells treated with DMSO. All C_t and ΔC_t values are shown in the Source Data files.

RNA metabolic labelling. Metabolic labelling was performed as previously described[44,45]. In brief, cells were treated with 200 μM 4-thiouridine (4sU; Sigma) for 1 h, followed by phenol–chloroform RNA extraction. RNA (80 μg) was incubated with biotin-HPDP (Thermo) to specifically biotinylate the newly transcribed 4sU-labelled RNAs. Biotinylated RNAs were then pulled down using the μMacs Streptavidin Kit (Miltenyi) and at least 100 ng of pulled down RNA was used for reverse transcription and downstream qPCR analysis. This experiment was performed once with two biological replicates.

Quantifying mRNA half-lives by transcription inhibition. Wild-type, *Fermt2* knockout, *Rela* knockout and *Actg1* knockout cells were treated with 10 μg ml^{-1} actinomycin D (Sigma) to block transcription. Cells were then collected in TRIzol 0, 1, 2, 4 and 8 h after treatment for RNA extraction. *Rn18s* was used as a housekeeping gene, as its expression level was not affected over the time course of treatment (data not shown). Half-lives were then quantified from fitted nonlinear exponential decay curves.

Cytotoxicity assay. Approximately 7,000 cells were seeded per well in a 96-well plate and incubated with media containing 25 ng ml^{-1} of mouse TNF. Twenty-four hours later, cells were washed with PBS and incubated for 5 h with media containing 3 mg ml^{-1} 3-(4,5-dimethylthiazol-2-yl)-2,5-diphenyltetrazolium bromide (MTT). The formed formazan (the product of MTT metabolism by viable cells) was resuspended in a 50% DMSO:50% ethanol solution, and optical density (O.D.) was measured at 572 nm using a FLUOstar Omega spectrophotometer (BMGH Labtech). Per cent cytotoxicity was measured using the following formula: (O.D. DMSO − O.D. TNF)/O.D. DMSO. This experiment was performed once.

mESC staining. Cells were fixed with 4% paraformaldehyde for 15 min at room temperature, permeabilized with 0.3% Triton X-100 (in PBS) for 10 min and then incubated with 1:1,000 phalloidin-568 (Thermo) in 3% BSA for 1 h at room temperature. After 3 × 15 min washes with PBT (0.1% Triton X-100 in PBS), samples were counterstained for 5 min at room temperature with 1:5,000 DAPI (Sigma) and mounted for imaging with Dako fluorescent mounting medium. Images were obtained on a Zeiss LSM700 confocal microscope using an LD C-Apochromat 63×/1.15 W Corr M27 objective. Protrusion length was measured using ImageJ.

Immunostaining. Larvae (100 hpf) from *alcama*$^{promoter\text{-}less+/-}$ and *alcama* $^{\Delta 8+/-}$ incrosses were collected and fixed in 4% paraformaldehyde. After removing the fixative with washes in 0.1% Tween in PBS, larvae were incubated with 3 μg ml^{-1} proteinase K for 1 h then washed with 1% BSA, 1%DMSO and 0.5% Triton-X in PBS (PBDT) before being incubated for 2 h with phalloidin Alexa-568 (Invitrogen) at room temperature to label F-actin. They were then washed with 0.1% Tween in PBS and mounted for heart imaging. Images of the hearts were acquired using a Zeiss LSM880 Axio Examiner confocal microscope with a W Plan-Apochromat 20×/1.0 objective. The ventricle length, or long axis of the ventricle, was measured from the apex of the ventricle to the junction of the ventricle with the bulbus arteriosus using Zen Black. In the first experiment, larvae were genotyped after imaging.

alcama$^{promoter\text{-}less}$ larvae were obtained from F_2 heterozygous parents generated by outcrossing the founder and F_1 fish. *alcama* $^{\Delta 8}$ larvae were obtained from an incross of F_3 heterozygous parents generated by consecutive outcrosses.

Confocal microscopy. A Zeiss LSM 700 confocal microscope was used for live imaging of the trunk and brain vasculature in wild-type and *egfl7*$^{full\ locus\ del.}$, *vegfaa*$^{\Delta 10}$ and *vegfaa*$^{promoter\text{-}less}$ mutant embryos. Embryos were anaesthetized with a low dose of tricaine, placed in a glass-bottomed Petri dish (MatTek) on a layer of 1.2% low melt agarose and imaged using Plan-Apochromat 10×/0.45 and LCI Plan-Neofluar 25×/0.8 objectives. In wild-type embryos at 60 hpf, an average of 13 central arteries have connected to the basilar artery[46].

vegfaa$^{promoter\text{-}less}$ larvae were obtained from F_2 heterozygous parents generated by outcrossing the founder and F_1 fish.

To measure blood flow velocity, we performed time-lapse imaging of the trunk region of 78 hpf wild-type, maternal zygotic *hbegfa*$^{\Delta 7-/-}$ and maternal zygotic *hbegfa*$^{full\ locus\ del.-/-}$ larvae using a Zeiss Spinning disc CSU-X1 confocal microscope with a high-speed camera, and quantified blood flow velocity in the dorsal aorta by measuring the time needed for erythrocytes to move 200 μm at the level of the fifth and sixth somites, using Zen Blue (as previously described)[47].

hbegfa$^{full\ locus\ del.}$ larvae were obtained from F_2 homozygous parents generated by outcrossing the founder. *hbegfa*$^{\Delta 7}$ and *vegfaa*$^{\Delta 10}$ larvae were obtained from an incross of F_3 heterozygous parents that were generated by consecutive outcrosses.

Western blot analysis and antibodies. MKFs and MEFs were lysed in modified RIPA buffer (150 mM NaCl, 50 mM TrisHCl pH 7.4, 1% IGEPAL, 0.1% sodium deoxycholate, 1 mM EDTA) supplemented with protease inhibitors (cOmplete ULTRA Mini, Roche) and phenylmethylsulfonyl fluoride (PMSF). Protein samples of 35 μg were separated using sodium dodecyl sulfate polyacrylamide gel electrophoresis (SDS–PAGE) on precast TGX gradient gels (Biorad) (ACTB control was run on the same gel as a loading control) and then electrophoretically transferred to polyvinylidine fluoride membranes (Biorad) using a Transblot Turbo Transfer System (Biorad). Membranes for RELA or FERMT2 were blocked in 5% BSA (Sigma) or 5% non-fat milk (Sigma), respectively, for 1 h, then probed with primary antibodies overnight at 4 °C. The following day, membranes were probed with peroxidase-conjugated secondary antibodies for 1 h at room temperature. For analysis, membranes were incubated with enhanced chemiluminescence (ECL) substrate (Clarity Western ECL Substrate, Biorad) and imaged using a ChemiDoc MP system (Biorad). The following antibodies were used: FERMT2 (Millipore, MAB2617; clone 3A3, 1:1,000), RELA (Cell Signaling Technology, 6956, 1:1,000), ACTB (Cell Signaling Technology, 8457, 1:1,000), anti-mouse horseradish peroxidase (HRP)-conjugated IgG (Thermo, 31430, 1:10,000) and anti-rabbit HRP-conjugated IgG (Thermo, 31460, 1:10,000). This experiment was performed once.

Chromatin immunoprecipitation. ChIP was performed using the truChIP Chromatin Shearing Reagent kit (Covaris) using 30 million cells per immunoprecipitation according to the manufacturer's protocol. Chromatin was sheared using Bioruptor (Diagenode) to generate fragments of 200–400 bp in size. Immunoprecipitation was then performed as previously described[48]. The following antibodies were used: rabbit IgG (4 μg per immunoprecipitation, 026102, Thermo Fischer), WDR5 (4 μg per immunoprecipitation, 13105, Cell Signaling Technology) and H3K4me3 (4 μg per immunoprecipitation, 9751, Cell Signaling Technology). Following immunoprecipitation and reverse cross-linking, samples were purified using the NucleoSpin Gel and PCR Clean-up kit (Macherey-Nagel), according

to the manufacturer's protocol for samples containing sodium dodecyl sulfate. ChIP–qPCR experiments on *Rela* knockout cells where UPF1/EXOSC4 or XRN1 were knocked down were performed only once.

ATAC-seq material extraction and library preparation. Cells were trypsinized and washed with PBS. Counting of cells was performed with MOXI Z Mini Automated Cell Counter Kit (Orflo) and 50,000 cells were used for ATAC library preparation using the Tn5 transposase from the Nextera DNA Sample Preparation Kit (Illumina). The cell pellet was resuspended in 50 μl PBS and mixed with 25 μl tagmentation DNA (TD) buffer, 2.5 μl Tn5, 0.5 μl 10% NP-40 and 22 μl water. This mixture of Tn5 and cells was incubated at 37 °C for 30 min with occasional snap mixing. Transposase treatment was followed by 30 min incubation at 50 °C with 500 mM EDTA pH8.0 for optimal recovery of digested DNA fragments. For neutralization of EDTA, 100 μl of 50 mM $MgCl_2$ was added, followed by purification of the DNA fragments using the MinElute PCR Purification Kit (Qiagen). Amplification of the library together with indexing was performed as previously described[49]. Libraries were mixed in equimolar ratios and sequenced on a NextSeq500 platform using v2 chemistry.

ATAC-seq analysis. The samples were assessed for quality using FastQC (http://www.bioinformatics.babraham.ac.uk/projects/fastqc). Trimmomatic v.0.33[50] was used to trim reads after a quality drop below a mean of Q20 in a window of five nucleotides. Only reads above 30 nucleotides were cleared for further analyses. To normalize all samples to the same sequencing depth, 27 million reads per sample were randomly selected for further analysis. These reads were mapped against the Ensembl mouse genome version mm10 (GRCm38) with STAR 2.4.2a[51] using only unique alignments to exclude reads with unclear placing. The reads were further deduplicated using Picard 1.136 (http://broadinstitute.github.io/picard/) to avoid PCR artefacts leading to multiple copies of the same original fragment. The MACS2 peak caller v.2.1.0 was used to identify peaks. The minimum *q* value was set to −1.5 and the false discovery rate was changed to 0.01. To determine thresholds for significant peaks, the data were manually inspected in the Integrated Genomics Viewer (IGV) 2.3.52[52]. Peaks overlapping blacklisted regions (known mis-assemblies, satellite repeats) from ENCODE were excluded. To compare peaks between samples, the resulting lists of significant peaks were overlapped and unified to represent identical regions. After conversion of binary alignment map (BAM) files to bigWig format with deep Tools bamCoverage[53], the counts per unified peak per sample were computed with bigWigAverageOverBed (UCSC Genome Browser Utilities, http://hgdownload.cse.ucsc.edu/downloads.html). Raw counts for unified peaks were submitted to DESeq2 for normalization[54]. Spearman correlations were produced to identify the degree of reproducibility between samples using R. To allow a normalized display of samples in IGV, the raw BAM files were normalized for sequencing depth (number of mapped deduplicated reads per sample) and noise level (number of reads inside peaks). Two factors were computed and applied to the original BAM files using bedtools genomecov[55], resulting in normalized bigWig files for IGV.

RNA sequencing. RNA was isolated using the miRNeasy micro Kit (Qiagen). To avoid contamination with genomic DNA, samples were treated by on-column DNase digestion (DNase-Free DNase Set, Qiagen). Total RNA and library integrity were verified on LabChip Gx Touch 24 (Perkin Elmer). One microgram of the total RNA was used as input for the SMARTer Stranded Total RNA Sample Prep Kit–HI Mammalian (Clontech). RNA sequencing (RNA-seq) was performed on a NextSeq500 instrument (Illumina) using v2 chemistry, resulting in an average of 25 million–30 million reads per library, with 1 × 75 bp single-end setup.

RNA-seq analysis. The resulting raw reads were assessed for quality, adaptor content and duplication rates with FastQC. Reaper v.13-100 was used to trim reads after a quality drop below a mean of Q20 in a window of 10 nucleotides[56]. Only reads of at least 15 nucleotides were cleared for subsequent analyses. Trimmed and filtered reads were aligned against the Ensembl mouse genome version mm10 (GRCm38) using STAR 2.5.3a with the parameters '–outFilterMismatchNoverLmax 0.1–alignIntronMax 200000'[51]. The numbers of reads that aligned to genes were counted with featureCounts 1.6.0 from the Subread package[57]. Only reads mapping at least partially inside exons were admitted, and these reads were aggregated per gene. Reads overlapping with multiple genes or aligning to multiple regions were excluded. Differentially expressed genes were identified using DESeq2 v.1.14.1[58]. Genes were classified as significantly differentially expressed with $P < 0.05$ (Wald test), without assigning a specific minimum or maximum regulation fold change as transcriptional adaptation might not necessarily lead to strong upregulation levels. The Ensembl annotation was enriched with UniProt data (release 24 March 2017) based on Ensembl gene identifiers.

Sequence similarity and subsampling analyses. To identify similarity to one of the three query nucleotide sequences (*Fermt2*, *Actg1* and *Actb*), the longest respective transcript was selected (ENSMUST00000071555, ENSMUST00000045905 and ENSMUST00000100497) and compared to the whole genome using BLASTn[59]. Genes were defined to be similar to the mutated gene when a partial match was identified inside the target gene body or its promoter region (that is, 2 kb upstream of the TSS). Several alignment parameters were surveyed to identify the optimal degree of similarity. Alignment length, bit score and *E* value were queried to identify the dynamic range and optimal values using subsampling analyses (see below). *E* value denotes the probability that the match resulted by chance, when considering the whole target database (the genome in this case).

A subsampling approach was used to calculate a ranked *P* value for the significance of the percentage of upregulated genes in subsamples of a specific size (equivalent to the number of similar protein-coding genes) for each cell line model. In brief, the following algorithm was repeated 10,000 times: 1) get *X* random protein-coding genes, 2) calculate the percentage of upregulated genes in this subsample. The resulting list was filtered for subsamples with an equal or higher than expected number of upregulated genes according to a previous comparison (for example, for *Fermt2*, 18 protein-coding genes exhibit sequence similarity to its mRNA (= subsample size), 9 of which were also upregulated (= expectation)). The number of subsamples showing at least as many upregulated genes as the expectation represents the rank of the comparison. The ranked *P* value was computed by dividing that rank by the total number of iterations (= 10,000). Optimal thresholds varied for the different cell line models and ranged between 1) 20 and 180 nucleotides (alignment length); 2) 40 and 200 bit score (combination of alignment quality and length); and 3) 10 to 6.73×10^{-50} (maximum *E* value). We selected the following maximum *E* values from the optimal range for the follow-up similarity analyses: 5.1 for *Fermt2* and *Actg1*, and 2×10^{-48} for *Actb*. The much stricter *E* value for *Actb* was necessary because of its repetitive 3′UTR, which resulted in misleading 'noisy' matches. These *E*-value thresholds translate into local nucleotide sequence alignments that range from 24 to 1,901 nucleotides in length, with 75 to 96% identity.

Sequence alignments of *hif1ab*, *Actb* and *epas1a*. The BLASTn alignments of the longest transcript of *hif1ab* (ENSDART00000018500) with the *epas1a* gene body including its promoter (2 kb upstream of TSS) were visualized using Kablammo[60] at word size 7 and an *E* value of 25 (Extended Data Fig. 8f). Two additional alignments were performed to show homologous regions of the synthetic *hif1ab* transcript compared to 1) the original source transcript (ENSDART00000018500), using MUSCLE[61]; and 2) *epas1a*, including its promoter (TSS-2000), using BLASTn. The uncapped RNA composed solely of the *hif1ab* sequences that are similar to *epas1a* is 1,277 nucleotides in length, and the uncapped RNA composed solely of the *hif1ab* sequences that are not similar to *epas1a* is 1,929 nucleotides in length. The similarity of the coding sequences of zebrafish *actb1* transcript ENSDART00000054987 (query) to the mouse *Actb* transcript ENSMUST00000100497 (subject) was assessed with a MUSCLE alignment. All of these alignments can be found in the Supplementary Data.

Gene-set enrichment analyses. Genes that were strongly upregulated in all three knockout samples versus their respective wild-type samples ($P < 0.05$ (Wald test), $\log_2$(gene expression level in knockout cells/gene expression level in wild-type cells) (hereafter referred to as L2F) >0.585) were used for gene-set enrichment analyses using KOBAS[62].

Reporting summary. Further information on research design is available in the Nature Research Reporting Summary linked to this paper.

Data availability

ATAC-seq and RNA-seq data were deposited to the Gene Expression Omnibus (GEO) under accession codes GSE107075 and GSE114212.

30. Gerri, C. et al. Hif-1α regulates macrophage-endothelial interactions during blood vessel development in zebrafish. *Nat. Commun.* **8**, 15492 (2017).
31. Rossi, A. et al. Regulation of Vegf signaling by natural and synthetic ligands. *Blood* **128**, 2359–2366 (2016).
32. Lawson, N. D. & Weinstein, B. M. *In vivo* imaging of embryonic vascular development using transgenic zebrafish. *Dev. Biol.* **248**, 307–318 (2002).
33. Proulx, K., Lu, A. & Sumanas, S. Cranial vasculature in zebrafish forms by angioblast cluster-derived angiogenesis. *Dev. Biol.* **348**, 34–46 (2010).
34. Labun, K., Montague, T. G., Gagnon, J. A., Thyme, S. B. & Valen, E. CHOPCHOP v2: a web tool for the next generation of CRISPR genome engineering. *Nucleic Acids Res.* **44**, W272–W276 (2016).
35. Cermak, T. et al. Efficient design and assembly of custom TALEN and other TAL effector-based constructs for DNA targeting. *Nucleic Acids Res.* **39**, e82 (2011).
36. Doyle, E. L. et al. TAL effector specificity for base 0 of the DNA target is altered in a complex, effector- and assay-dependent manner by substitutions for the tryptophan in cryptic repeat −1. *PLoS One* **8**, e82120 (2013).
37. Gagnon, J. A. et al. Efficient mutagenesis by Cas9 protein-mediated oligonucleotide insertion and large-scale assessment of single-guide RNAs. *PLoS One* **9**, e98186 (2014).
38. Vejnar, C. E., Moreno-Mateos, M. A., Cifuentes, D., Bazzini, A. A. & Giraldez, A. J. Optimized CRISPR–Cas9 system for genome editing in zebrafish. Cold Spring Harb. Protoc. https://doi.org/10.1101/pdb.prot086850 (2016).
39. Theodosiou, M. et al. Kindlin-2 cooperates with talin to activate integrins and induces cell spreading by directly binding paxillin. *eLife* **5**, e10130 (2016).

40. Gapuzan, M. E., Yufit, P. V. & Gilmore, T. D. Immortalized embryonic mouse fibroblasts lacking the RelA subunit of transcription factor NF-κB have a malignantly transformed phenotype. *Oncogene* **21**, 2484–2492 (2002).
41. Ran, F. A. et al. Genome engineering using the CRISPR–Cas9 system. *Nat. Protoc.* **8**, 2281–2308 (2013).
42. Thakore, P. I. et al. Highly specific epigenome editing by CRISPR–Cas9 repressors for silencing of distal regulatory elements. *Nat. Methods* **12**, 1143–1149 (2015).
43. Martin, L. et al. Identification and characterization of small molecules that inhibit nonsense-mediated RNA decay and suppress nonsense p53 mutations. *Cancer Res.* **74**, 3104–3113 (2014).
44. Rädle, B. et al. Metabolic labeling of newly transcribed RNA for high resolution gene expression profiling of RNA synthesis, processing and decay in cell culture. *J. Vis. Exp.* **78**, e50195 (2013).
45. Sun, W. & Chen, W. Metabolic labeling of newly synthesized RNA with 4sU to in parallel assess RNA transcription and decay. *Methods Mol. Biol.* **1720**, 25–34 (2018).
46. Vanhollebeke, B. et al. Tip cell-specific requirement for an atypical Gpr124- and Reck-dependent Wnt/β-catenin pathway during brain angiogenesis. *eLife* **4**, e06489 (2015).
47. Kwon, H. B. et al. In vivo modulation of endothelial polarization by Apelin receptor signalling. *Nat. Commun.* **7**, 11805 (2016).
48. Blecher-Gonen, R. et al. High-throughput chromatin immunoprecipitation for genome-wide mapping of in vivo protein-DNA interactions and epigenomic states. *Nat. Protoc.* **8**, 539–554 (2013).
49. Buenrostro, J. D., Giresi, P. G., Zaba, L. C., Chang, H. Y. & Greenleaf, W. J. Transposition of native chromatin for fast and sensitive epigenomic profiling of open chromatin, DNA-binding proteins and nucleosome position. *Nat. Methods* **10**, 1213–1218 (2013).
50. Bolger, A. M., Lohse, M. & Usadel, B. Trimmomatic: a flexible trimmer for Illumina sequence data. *Bioinformatics* **30**, 2114–2120 (2014).
51. Dobin, A. et al. STAR: ultrafast universal RNA-seq aligner. *Bioinformatics* **29**, 15–21 (2013).
52. Robinson, J. T. et al. Integrative genomics viewer. *Nat. Biotechnol.* **29**, 24–26 (2011).
53. Ramírez, F., Dündar, F., Diehl, S., Grüning, B. A. & Manke, T. deepTools: a flexible platform for exploring deep-sequencing data. *Nucleic Acids Res.* **42**, W187–W191 (2014).
54. Anders, S. & Huber, W. Differential expression analysis for sequence count data. *Genome Biol.* **11**, R106 (2010).
55. Quinlan, A. R. & Hall, I. M. BEDTools: a flexible suite of utilities for comparing genomic features. *Bioinformatics* **26**, 841–842 (2010).
56. Davis, M. P., van Dongen, S., Abreu-Goodger, C., Bartonicek, N. & Enright, A. J. Kraken: a set of tools for quality control and analysis of high-throughput sequence data. *Methods* **63**, 41–49 (2013).
57. Liao, Y., Smyth, G. K. & Shi, W. featureCounts: an efficient general purpose program for assigning sequence reads to genomic features. *Bioinformatics* **30**, 923–930 (2014).
58. Love, M. I., Huber, W. & Anders, S. Moderated estimation of fold change and dispersion for RNA-seq data with DESeq2. *Genome Biol.* **15**, 550 (2014).
59. Altschul, S. F., Gish, W., Miller, W., Myers, E. W. & Lipman, D. J. Basic local alignment search tool. *J. Mol. Biol.* **215**, 403–410 (1990).
60. Wintersinger, J. A. & Wasmuth, J. D. Kablammo: an interactive, web-based BLAST results visualizer. *Bioinformatics* **31**, 1305–1306 (2015).
61. Edgar, R. C. MUSCLE: a multiple sequence alignment method with reduced time and space complexity. *BMC Bioinformatics* **5**, 113 (2004).
62. Xie, C. et al. KOBAS 2.0: a web server for annotation and identification of enriched pathways and diseases. *Nucleic Acids Res.* **39**, W316–W322 (2011).

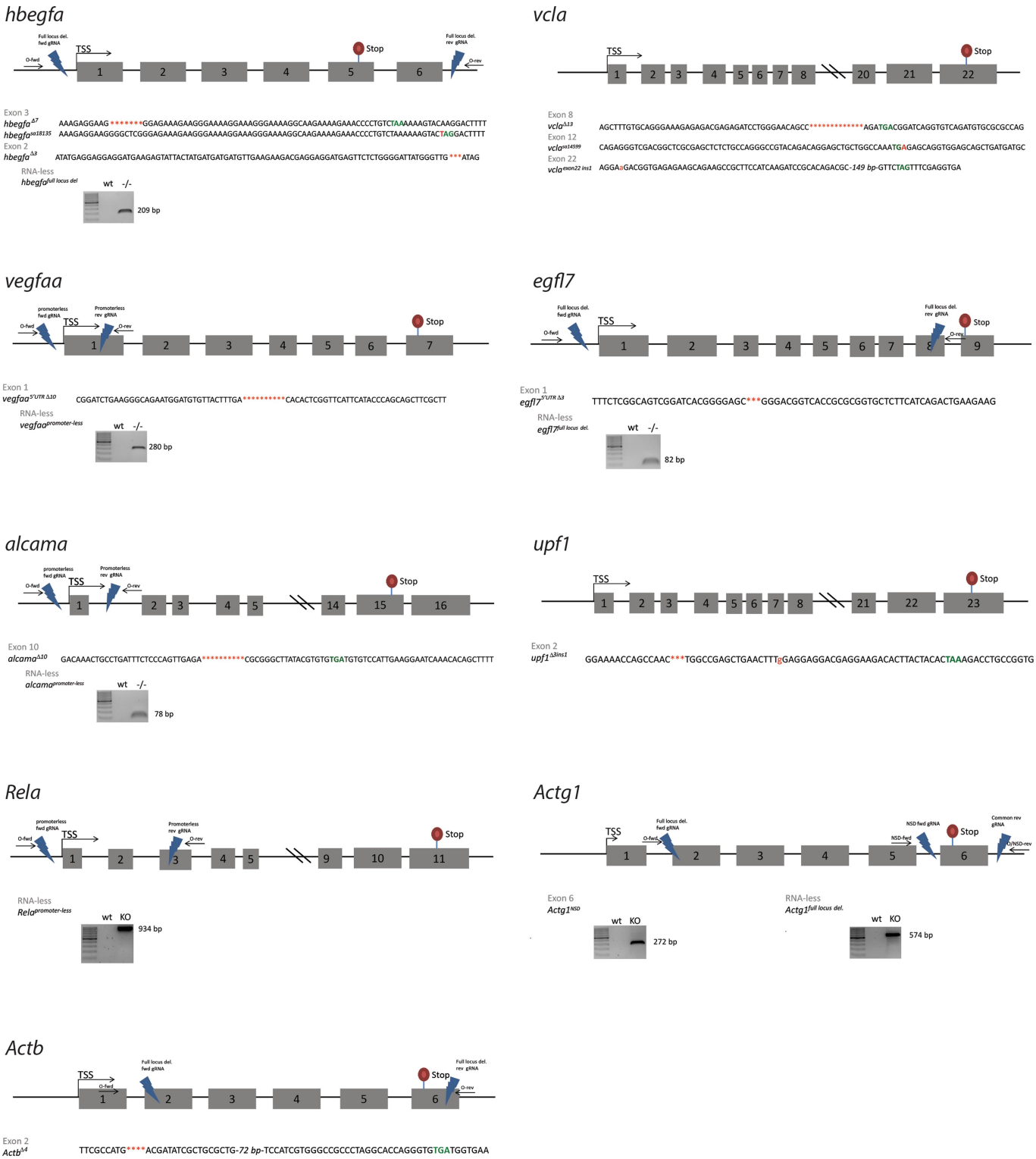

Extended Data Fig. 1 | Schematic illustration of the mutant alleles generated for this study. Partial DNA sequences of the different mutant alleles generated for this study, and images of gels providing evidence for deletions in RNA-less alleles. Red indicates mutation (asterisks, deletion; upper-case letters, substitution; lower-case letters, insertion); green indicates stop codon in alleles with a PTC; arrows indicate genotyping primers.

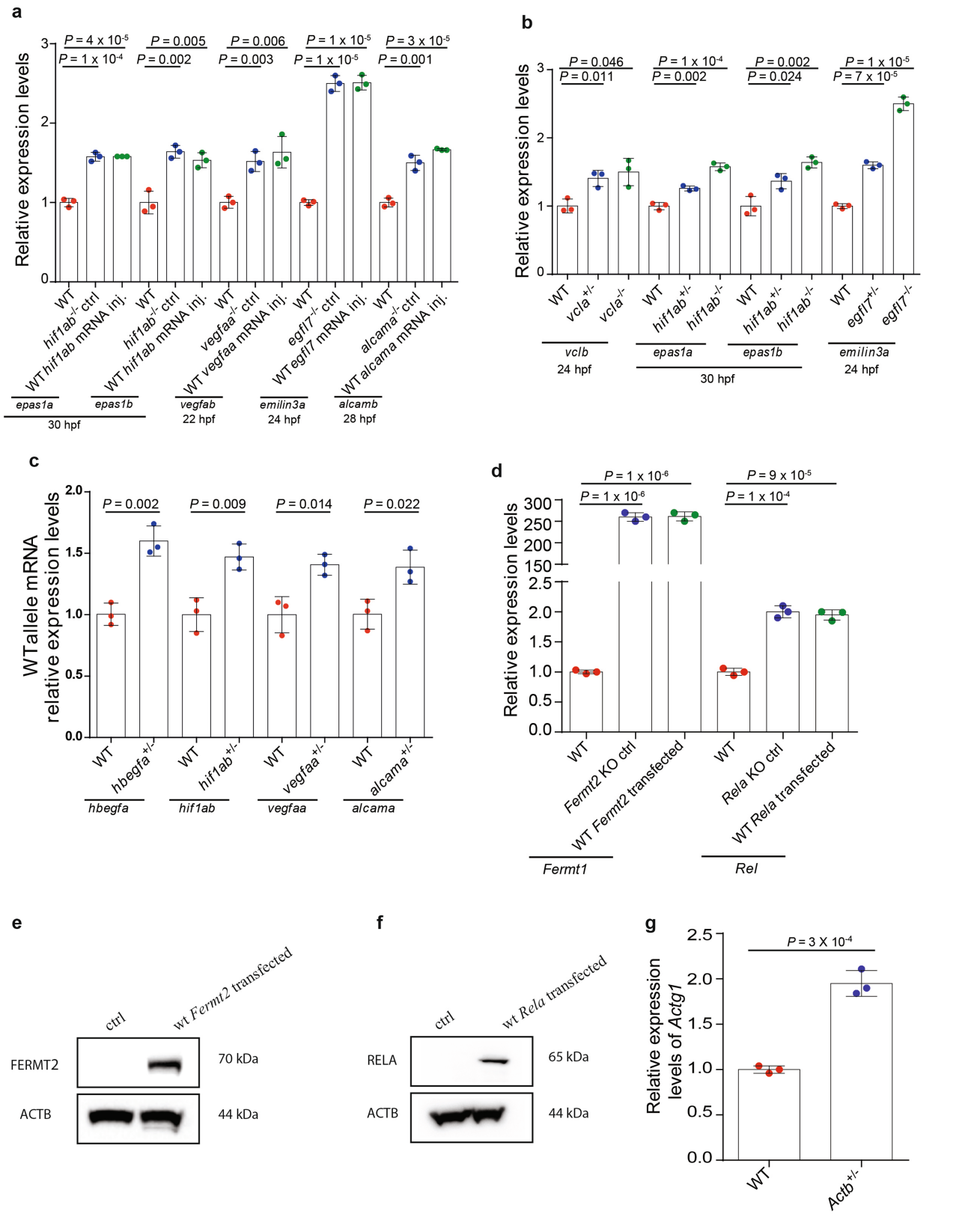

Extended Data Fig. 2 | See next page for caption.

Extended Data Fig. 2 | Transcriptional adaptation is independent of the loss of protein function. a, qPCR analysis of *epas1a*, *epas1b*, *vegfab*, *emilin3a* and *alcamb* mRNA expression levels in wild-type and *hif1ab*, *vegfaa*, *egfl7* and *alcama* mutant embryos injected (inj.) with *eGFP* mRNA (control; ctrl) or wild-type *hif1ab*, *vegfaa*, *egfl7* or *alcama* mRNA. **b**, qPCR analysis of *vclb*, *epas1a*, *epas1b* and *emilin3a* mRNA expression levels in *vcla*, *hif1ab* and *egfl7* wild-type, heterozygous and mutant zebrafish. **c**, qPCR analysis of *hbegfa*, *hif1ab*, *vegfaa* and *alcama* mRNA expression levels in *hbegfa*, *hif1ab*, *vegfaa* and *alcama* wild-type and heterozygous zebrafish, using primers specific for the wild-type allele. **d**, qPCR analysis of *Fermt1* and *Rel* mRNA expression levels in wild-type and *Fermt2* and *Rela* knockout cells transfected with empty vectors (control) or plasmids encoding wild-type FERMT2 or RELA. **e**, Western blot analysis of FERMT2 and ACTB levels in *Fermt2* knockout cells transfected with empty vectors (control) or plasmids encoding wild-type FERMT2. **f**, Western blot analysis of RELA and ACTB levels in *Rela* knockout cells transfected with empty vectors (control) or plasmids encoding wild-type RELA. **g**, qPCR analysis of *Actg1* mRNA expression levels in wild-type and heterozygous *Actb* mESCs. $n = 3$ biologically independent samples. Wild-type or control expression levels were set at 1 for each assay. Data are mean ± s.d., and a two-tailed Student's *t*-test was used to calculate *P* values (**a**–**d**, **g**). The experiments in **e**, **f** were performed only once. For the source data for western blots, see Supplementary Fig. 1.

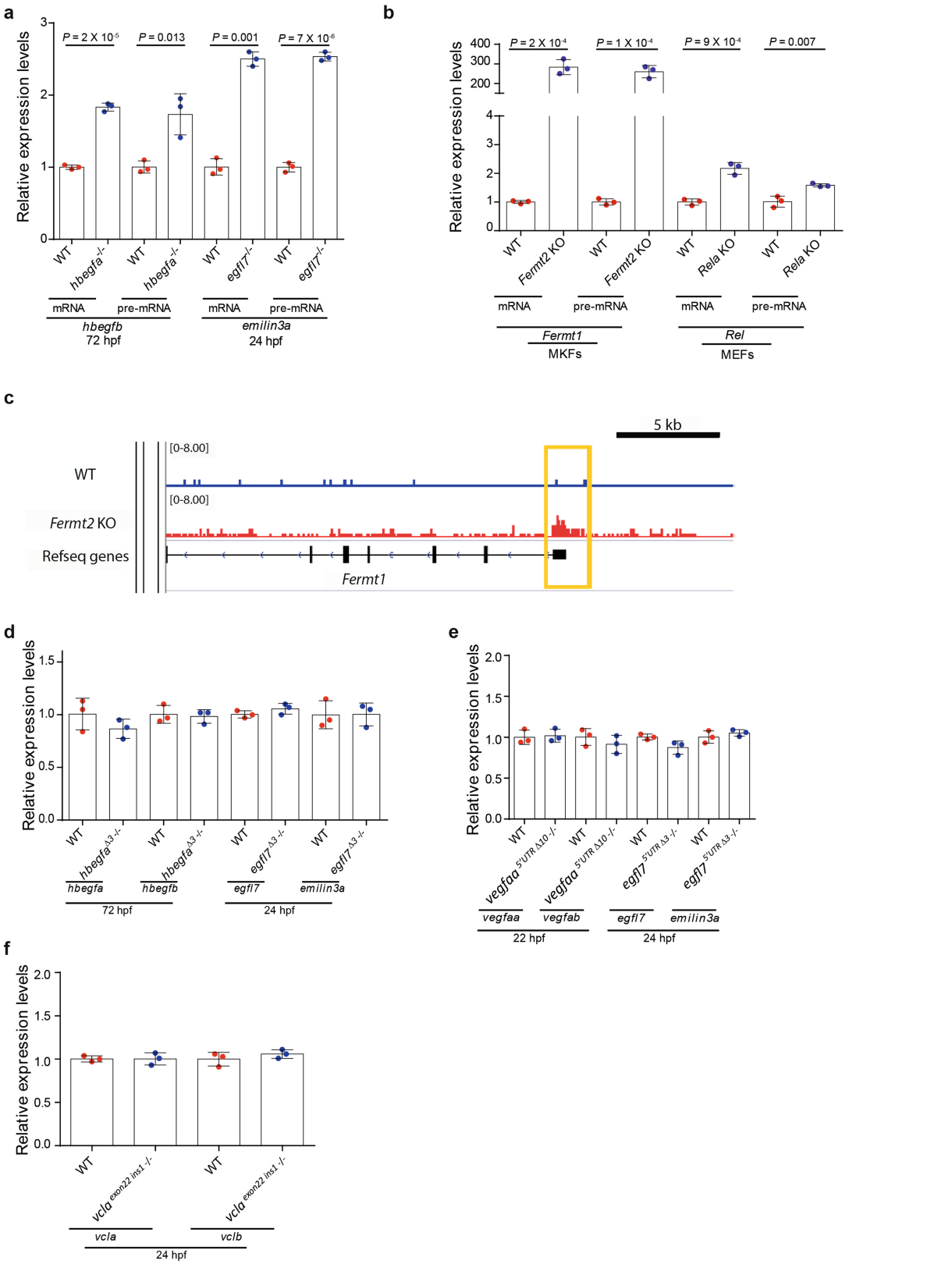

Extended Data Fig. 3 | Transcriptional adaptation involves enhanced transcription and is independent of the DNA lesion itself. a, qPCR analysis of *hbegfb* and *emilin3a* mRNA and pre-mRNA expression levels in *hbegfa* and *egfl7* wild-type and mutant zebrafish. **b**, qPCR analysis of *Fermt1* and *Rel* mRNA and pre-mRNA expression levels in *Fermt2* and *Rela* wild-type and knockout cells. **c**, IGV tracks of the *Fermt1* locus showing ATAC-seq signals in wild-type and *Fermt2* knockout cells. **d**, qPCR analysis of *hbegfa*, *hbegfb*, *egfl7* and *emilin3a* mRNA expression levels in *hbegfa* and *egfl7* wild-type and Δ3 mutant zebrafish. **e**, qPCR analysis of *vegfaa*, *vegfab*, *egfl7* and *emilin3a* mRNA expression levels in *vegfaa* and *egfl7* wild-type and 5′UTR mutant zebrafish. **f**, qPCR analysis of *vcla* and *vclb* mRNA expression levels in *vcla* wild-type and last exon (exon 22) mutant zebrafish. $n = 3$ biologically independent samples. Wild-type expression levels were set at 1 for each assay. Data are mean ± s.d., and a two-tailed Student's *t*-test was used to calculate *P* values.

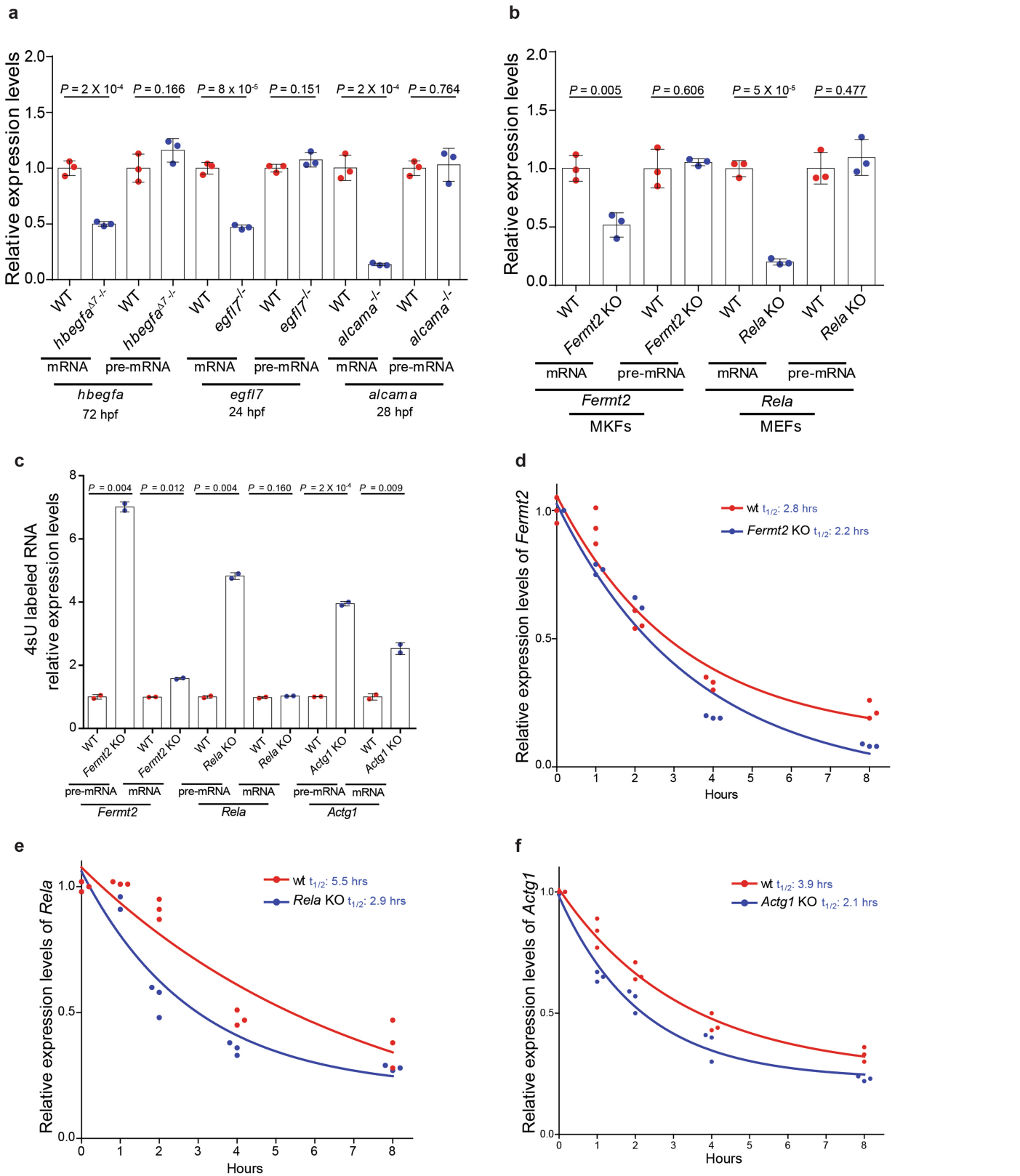

Extended Data Fig. 4 | Reduction in mutant transcript levels is caused by mRNA decay. a, qPCR analysis of *hbegfa*, *egfl7* and *alcama* mRNA and pre-mRNA expression levels in *hbegfa*, *egfl7* and *alcama* wild-type and mutant zebrafish. **b**, qPCR analysis of *Fermt2* and *Rela* mRNA and pre-mRNA expression levels in *Fermt2* and *Rela* wild-type and knockout cells. **c**, qPCR analysis of 4sU-labelled *Fermt2*, *Rela* and *Actg1* mRNA and pre-mRNA expression levels in *Fermt2*, *Rela* and *Actg1* wild-type and knockout cells. **d**, Fitted exponential decay curves of *Fermt2* mRNA expression levels in wild-type and *Fermt2* knockout cells. $t_{1/2}$, half-life. **e**, Fitted exponential decay curves of *Rela* mRNA expression levels in wild-type and *Rela* knockout cells. **f**, Fitted exponential decay curves of *Actg1* mRNA expression levels in wild-type and *Actg1* knockout cells. $n = 3$ (**a**, **b**, **d**–**f**) or $n = 2$ (**c**) biologically independent samples. Wild-type expression levels were set at 1 for each assay (a–c). Data are mean ± s.d., and a two-tailed Student's *t*-test was used to calculate *P* values.

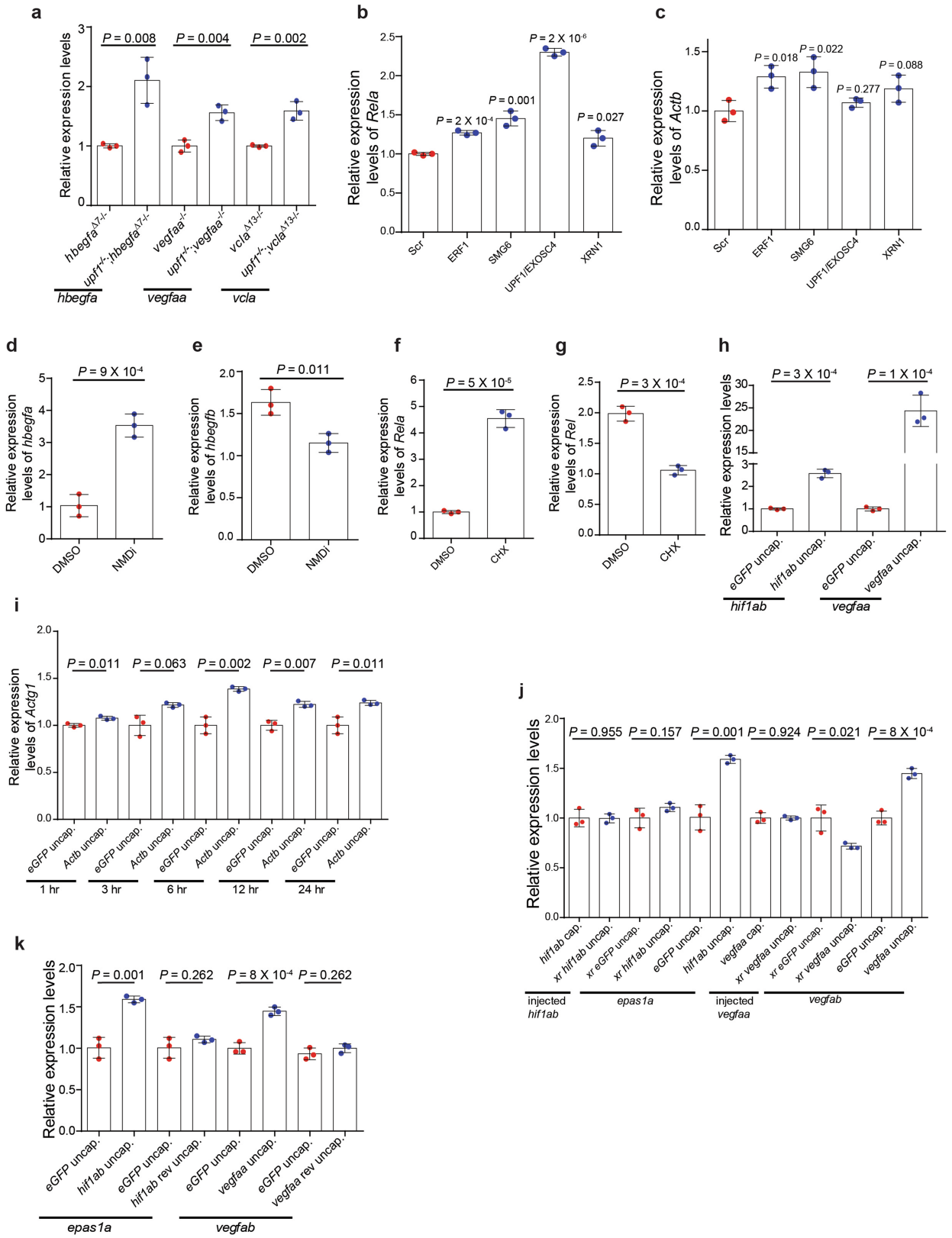

Extended Data Fig. 5 | See next page for caption.

Extended Data Fig. 5 | RNA decay induces transcriptional adaptation. **a**, qPCR analysis of *hbegfa*, *vegfaa* and *vcla* mRNA expression levels in *upf1;hbegfa*, *upf1;vegfaa* and *upf1*;*vcla* double mutant zebrafish. **b**, qPCR analysis of *Rela* mRNA expression levels after siRNA-mediated knockdown of the indicated proteins in *Rela* knockout cells. **c**, qPCR analysis of *Actb* mRNA expression levels after siRNA-mediated knockdown of the indicated proteins in *Actb* knockout cells. **d**, qPCR analysis of *hbegfa* mRNA expression levels in 6 dpf *hbegfa* mutants treated with NMD inhibitor (NMDi). **e**, qPCR analysis of *hbegfb* mRNA expression levels in 6 dpf *hbegfa* mutants treated with NMDi. **f**, qPCR analysis of *Rela* mRNA expression levels in *Rela* knockout cells treated with cycloheximide (CHX). **g**, qPCR analysis of *Rel* mRNA expression levels in *Rela* knockout cells treated with CHX. **H**, qPCR analysis of endogenous *hif1ab* and *vegfaa* mRNA expression levels in 6 hpf wild-type embryos injected with uncapped *hif1ab* or *vegfaa* RNA. **I**, qPCR analysis of *Actg1* mRNA expression levels in mESCs transfected with uncapped *Actb* RNA at different times after transfection. **j**, qPCR analysis of injected *hif1ab*, *epas1a*, injected *vegfaa* and *vegfab* RNA expression levels in 6 hpf wild-type embryos injected with uncapped *hif1ab* or *vegfaa* transcripts with or without a 5′ XRN1-resistant (xr) sequence. **k**, qPCR analysis of *epas1a* and *vegfab* mRNA expression levels in 6 hpf wild-type zebrafish embryos injected with uncapped sense or antisense (rev) *hif1ab* or *vegfaa* RNA; the same *eGFP* uncap. control samples were used for the *epas1a* experiments. Wild-type or control expression levels were set at 1 for each assay (**a**–**d**, **f**, **h**–**k**). $n = 3$ biologically independent samples. Data are mean ± s.d., and a two-tailed Student's *t*-test was used to calculate *P* values.

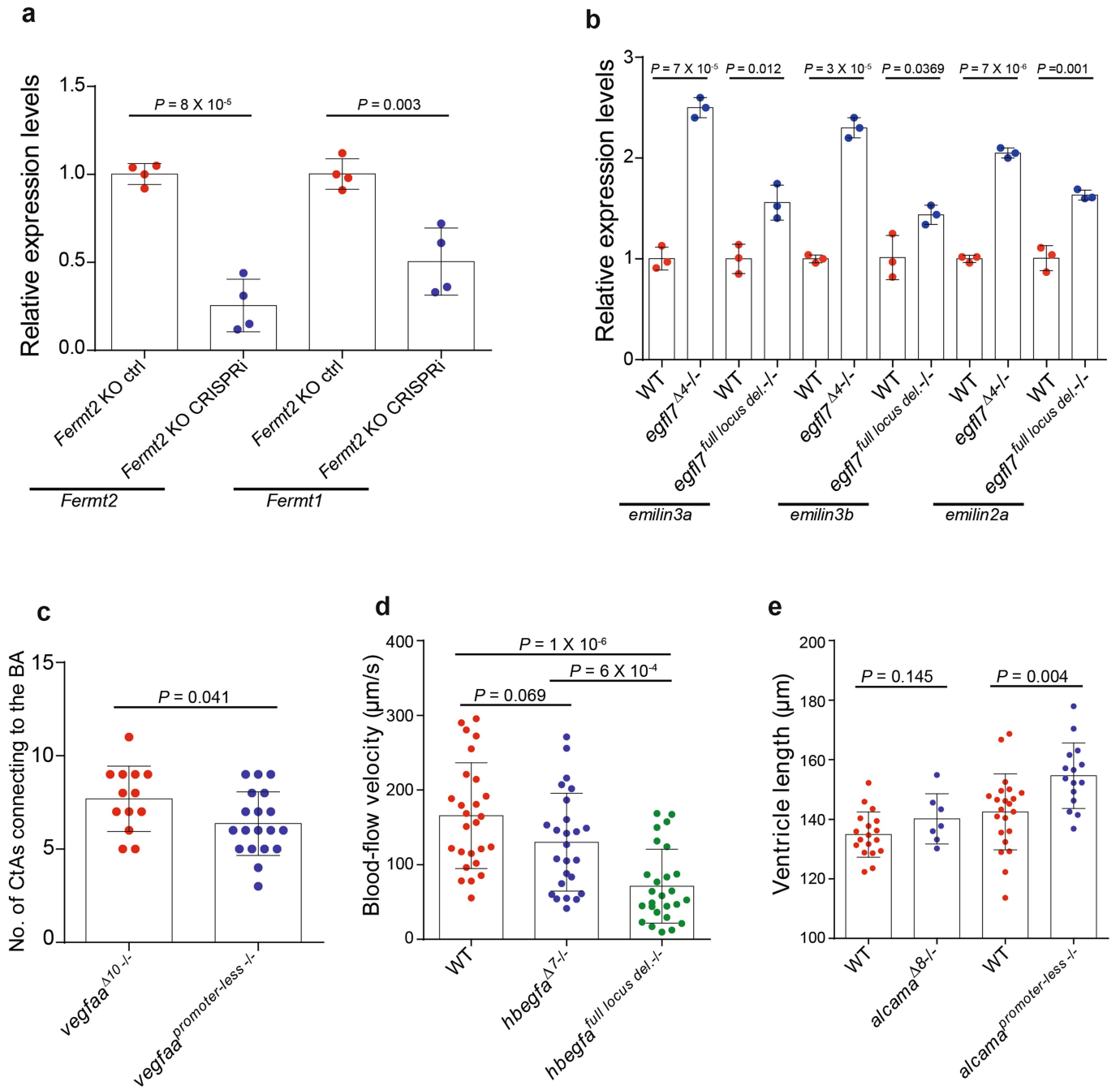

Extended Data Fig. 6 | Mutant mRNA decay helps confer genetic robustness. a, qPCR analysis of *Fermt2* and *Fermt1* mRNA expression levels following CRISPR interference-mediated knockdown of *Fermt2* transcription in *Fermt2* knockout cells. **b**, qPCR analysis of *emilin3a*, *emilin3b* and *emilin2a* mRNA expression levels in 20 hpf wild types, *egfl7*$^{\Delta 4}$ mutants and *egfl7*$^{full\ locus\ del.}$ mutants. **c**, Number of central arteries (CtAs) connecting to the basilar artery (BA) in 58 hpf *vegfaa*$^{\Delta 10}$ and *vegfaa*$^{promoter\text{-}less}$ mutants. **d**, Blood-flow velocity in 78 hpf wild types, *hbegfa*$^{\Delta 7}$ mutants and *hbegfa*$^{full\ locus\ del.}$ mutants. **e**, Quantification of the cardiac ventricle length in 100 hpf wild types, *alcama* $^{\Delta 8}$ mutants and *alcama*$^{promoter\text{-}less}$ mutants. Wild-type or control expression levels were set at 1 for each assay (**a**, **b**). $n = 3$ (**a**, **b**); $n = 13$ (*vegfaa*$^{\Delta 10-/-}$) and 19 (*vegfaa*$^{promoter\text{-}less-/-}$) (**c**); $n = 25$ (**d**); and $n = 18$ (wild-type siblings of *alcama*$^{\Delta 8-/-}$), 7 (*alcama*$^{\Delta 8-/-}$), 22 (wild-type siblings of *alcama*$^{promoter\text{-}less-/-}$) and 15 (*alcama*$^{promoter\text{-}less-/-}$) (**e**) animals. Data are mean ± s.d., and a two-tailed Student's *t*-test was used to calculate *P* values.

a

	No. of upregulated genes L2F > 0.585	No. of upregulated genes L2F KO >WT	No. of downregulated genes L2F < -0.585	No. of downregulated genes L2F KO <WT
Fermt2 KO	2,002	3,634	2,237	3,935
Actg1 KO	2,081	3,509	1,225	2,652
Actb KO	584	1,155	703	1,110

b

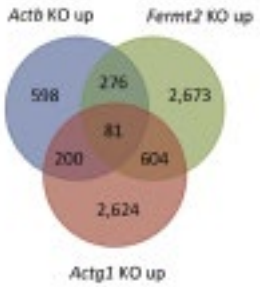

c

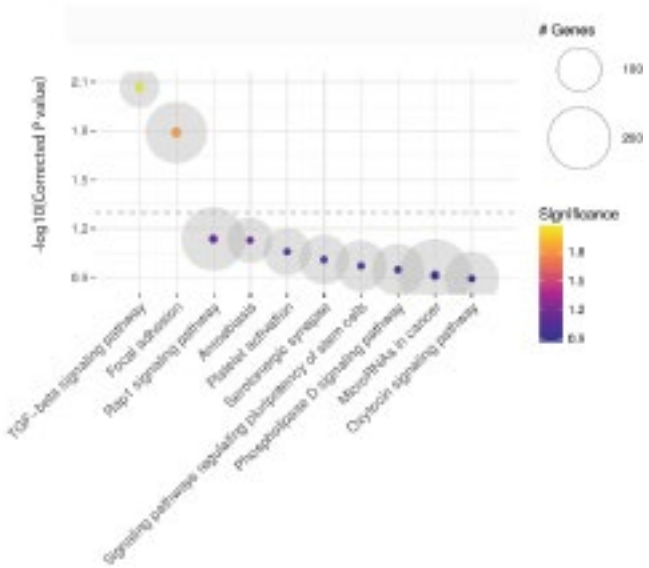

d

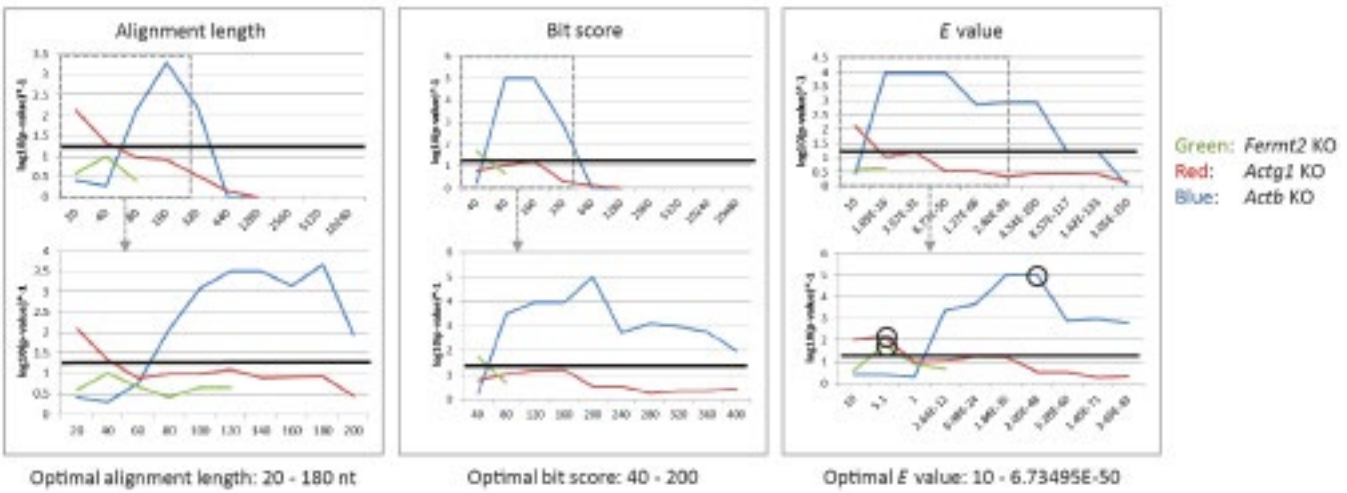

Extended Data Fig. 7 | Analysis of sequence similarity parameters in models of transcriptional adaptation. a, Numbers of differentially expressed genes in the different knockout cell line models; $P \leq 0.05$; these genes are distributed throughout the genome (data not shown). **b**, Venn diagram of genes upregulated in the three different cell line models with L2F knockout > wild-type and $P \leq 0.05$. **c**, KEGG pathway enrichment analysis for genes commonly upregulated in *Fermt2*, *Actg1* and *Actb* knockout compared to wild-type cells. The top ten pathways based on *P* value are displayed. The dashed line marks a *P* value of 0.05. Circle sizes provide an estimation of scale; outer grey circles represent the total number of genes in the pathway; and centred coloured circles represent the number of genes in the pathway that are commonly upregulated. **d**, Impact of various values of three different BLASTn alignment-quality parameters (alignment length, bit score and *E* value) on the significance of the observed correlation between upregulation and sequence similarity, and therefore the identification or prediction of putative adapting genes. The *E* value describes the probability of the match resulting from chance (a lower value corresponds to a lower probability), and the bit score evaluates the combination of alignment quality and length (a higher value corresponds to a better alignment).The *y* axis of each diagram shows the negative $\log_{10}$ of the *P* value and the *x* axis shows the respective parameter value. A *P* value of 0.05 is marked with a black horizontal line. The *E* value thresholds used in our analyses are highlighted with a circle. Lines ending preliminarily indicate a lack of any remaining alignments after that point. The first row of diagrams explores large variations of thresholds, in an attempt to identify the total range, whereas the second row focuses on the most relevant window for the three genes investigated. The optimal thresholds differ considerably depending on the gene analysed. $n = 2$ biologically independent samples. *P* value was computed by bootstrapping random subsamples (see the 'Sequence similarity and subsampling analyses' section of the Methods). *P* values were not corrected for multiple testing.

a

Gene	L2F Fermt2 KO/wt	Pval	Padj
Fermt1	8.055307305	5.19E-43	1.94E-41
Dchs2	3.501304705	4.92E-11	3.99E-10
Paqr5	1.679449433	2.46E-13	2.41E-12
Mixipl	0.618877214	0.409259	0.573342
Pcnx	0.502076808	8.12E-06	3.76E-05
Nkain1	0.39205614	0.043898	0.097439
Vapb	0.386807243	2.47E-06	1.22E-05
Strbp	0.273294934	0.000195	0.000738
Prkar2b	0.271409666	0.006358	0.017971
Pou2f1	0.191075348	0.041339	0.092619
Depdc1b	0.097436998	0.581669	0.726092
Fermt3	0.035722034	0.948806	0.970063
Mfsd11	-0.085901914	0.621497	0.757444
Trim24	-0.255516547	0.00941	0.025447
Atm	-0.516886899	3.84E-13	3.70E-12
Slc25a13	-0.678800185	1.40E-06	7.14E-06
Abhd18	-0.82015185	0.024339	0.05872
Eda	-1.503214668	0.167483	0.294635

b

Gene	L2F Actg1 KO/wt	Pval	Padj
Actg2	5.86	0	0
Ptp4a3	3.91	0.00000246	1.40E-05
Hcn1	3.47	1.84E-09	1.45E-08
Adamts12	2.14	4.91E-46	2.53E-44
Sec24d	0.81	4.36E-20	7.67E-19
Acta2	0.76	6.48E-45	3.22E-43
Hcfc2	0.72	2.91E-08	2.05E-07
Ubap1l	0.45	0.573535144	0.743877533
Pde10a	0.44	0.000216157	0.000933738
Nol11	0.43	9.8E-11	8.69E-10
Actr1b	0.29	0.000631774	0.002508725
Atf7	0.29	0.002212762	0.007853264
Actb	0.19	0.000162494	0.00071632
Znrf2	0.13	0.270233353	0.458179229
Lrrc58	-0.15	0.019456235	0.054271242
Fmnl2	-0.2	0.008174843	0.025396546
Cdk12	-0.24	0.000463124	0.001889135
Actr1a	-0.28	0.000780469	0.003040052
Fbxl17	-0.49	0.00000017	0.000284708
Grpel2	-0.58	0.0000601	0.45255246
Acta1	-1.91	1.01E-25	2.36E-24

c

Gene	L2F Actb KO/wt	Pval	Padj
Acta2	7.948538835	5.34E-151	7.98E-147
Actg2	2.961946198	0.020429	1
Acta1	2.556443324	0.001842	0.036378
Actc1	2.284580096	0.017007	1
Rasl2-9	1.353877161	0.350521	1
Actg1	0.982444337	3.78E-11	7.63E-09
Pde10a	0.552114557	0.432741	0.833262
Fbxl17	0.524667754	0.032681	0.244749
Gm17087	0.158304112	0.936537	0.989226
Lrrc58	0.028544142	0.851949	0.974102

d

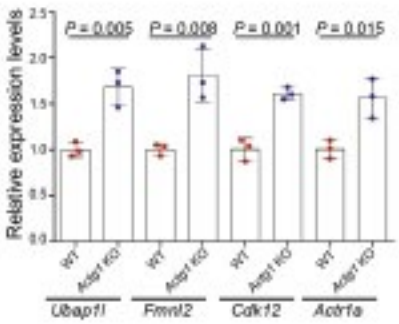

e

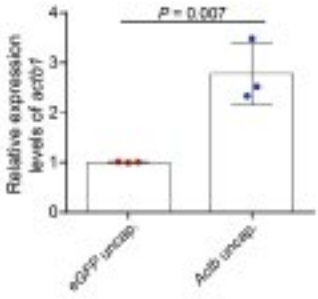

f

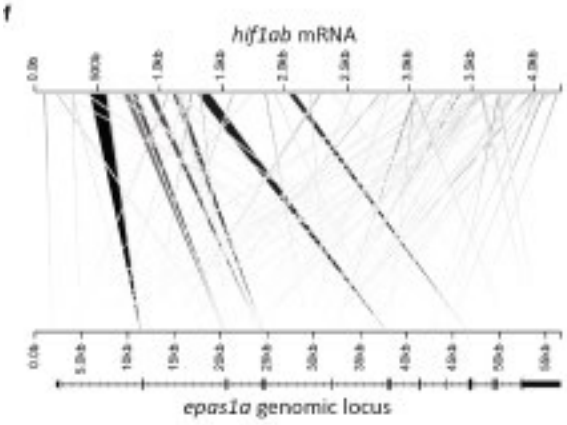

g

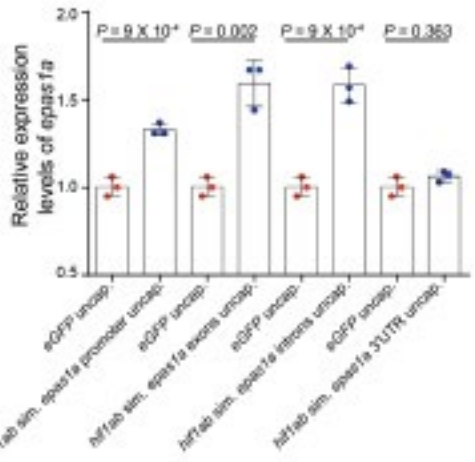

Extended Data Fig. 8 | See next page for caption.

Extended Data Fig. 8 | Expression level of genes exhibiting sequence similarity in the different mouse cell line models. a–c, RNA-seq analysis of genes exhibiting sequence similarity with *Fermt2* (**a**), *Actg1* (**b**) or *Actb* (**c**) in knockout compared to wild-type cells. Bold, significantly upregulated in knockout relative to wild-type cells; red, L2F>0, blue, L2F<0; green, *P* value or adjusted *P* value ≤ 0.05; purple; genes exhibiting sequence similarity with the mutated gene's mRNA in their promoter region; yellow, genes exhibiting sequence similarity with the mutated gene's mRNA in their 3′UTR region. Other non-coloured genes exhibit sequence similarity with the mutated gene's mRNA in their exons or introns. Boxed, upregulated in knockout but not RNA-less cells; no *Fermt2* RNA-less allele was analysed. **d**, qPCR analysis of *Ubapl*, *Fmnl2*, *Cdk12* and *Actr1a* pre-mRNA expression levels in *Actg1* knockout relative to wild-type cells. **e**, qPCR analysis of *actb1* mRNA expression levels in 6 hpf wild-type zebrafish injected with uncapped mouse *Actb* RNA. **f**, Schematic representation of regions of sequence similarity between *hif1ab* mRNA and the *epas1a* locus. Grey shaded triangles represent the alignments; intensity represents the alignment quality; and width at the base represents the length of the similarity region. **g**, qPCR analysis of *epas1a* mRNA expression levels in 6 hpf wild-type zebrafish embryos injected with uncapped RNA composed solely of the *hif1ab* sequences similar to the *epas1a* promoter, exons, introns or 3′UTR; the same *eGFP* uncap. control samples were used for all comparisons. $n = 2$ (**a–c**) or $n = 3$ (**d**, **e**, **g**) biologically independent samples. DESeq2 tests were used to test for significance of coefficients in a negative binomial generalized linear model with the Wald test (**a–c**). *P* values were not corrected for multiple testing. Wild-type or control expression levels were set at 1 for each assay (**d**, **e**, **g**). Data are mean ± s.d., and a two-tailed Student's *t*-test was used to calculate *P* values.

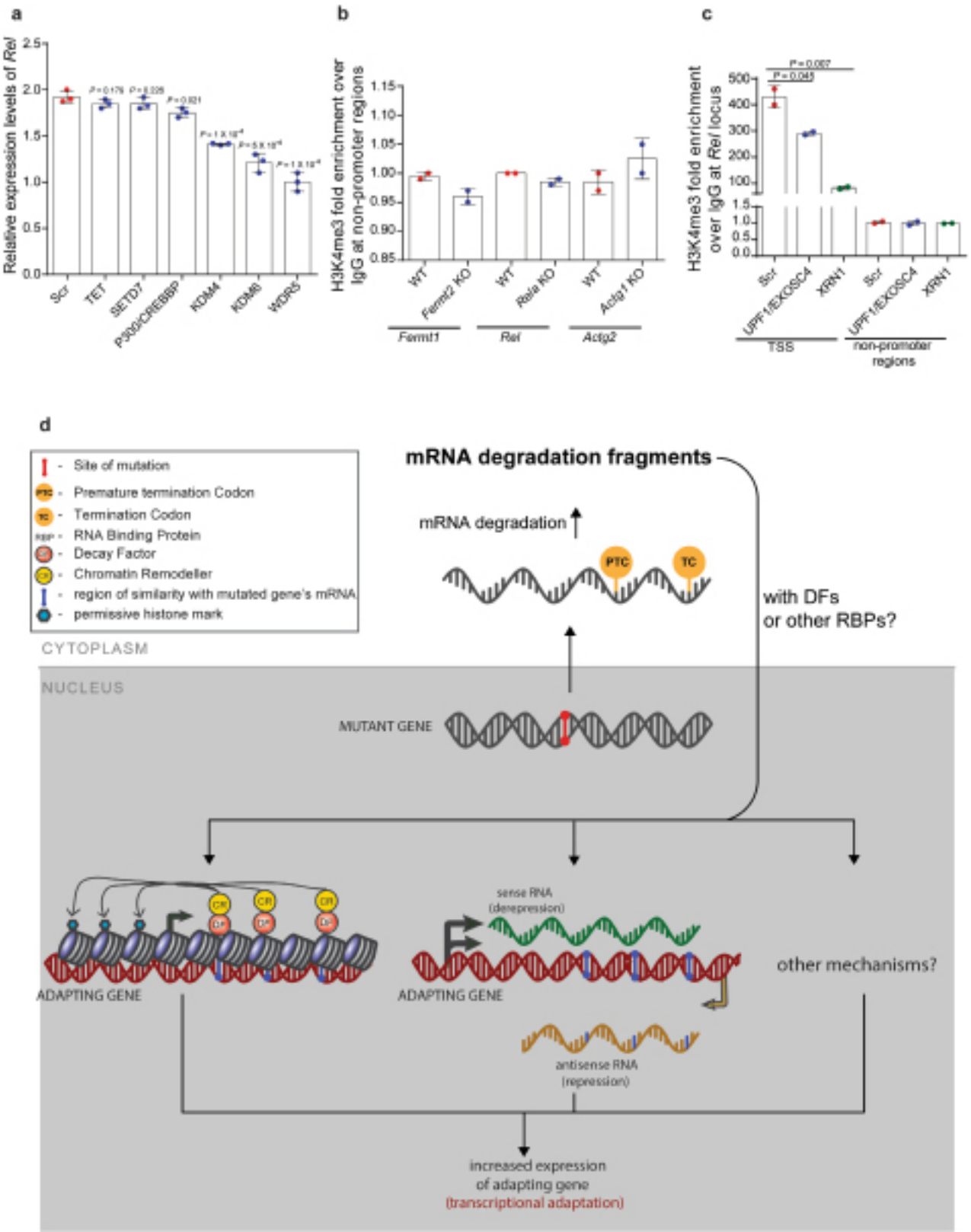

Extended Data Fig. 9 | See next page for caption.

Extended Data Fig. 9 | Transcriptional adaptation involves chromatin remodelling that is dependent on the activity of decay factors. a, qPCR analysis of *Rel* mRNA expression levels after siRNA-mediated knockdown of the indicated proteins in *Rela* knockout cells. **b**, ChIP–qPCR analysis of H3K4me3 occupancy at non-promoter regions (as a control) of *Fermt1*, *Rel* and *Actg2* in *Fermt*2, *Rela* and *Actg1* knockout cells, respectively, compared to wild-type cells. **c**, ChIP–qPCR analysis of H3K4me3 occupancy near the *Rel* TSS and a non-promoter region (as a control) after siRNA-mediated knockdown of the indicated proteins in *Rela* knockout cells. **d**, Current expanded model of transcriptional adaptation to mutations. RNA decay fragments may act as intermediates to bring decay factors and chromatin remodellers to adapting gene loci, thereby triggering increased gene expression. Alternatively, RNA decay fragments may function by repressing antisense RNAs at the adapting gene loci, thus allowing for increased sense mRNA expression. It is, however, likely that additional mechanisms are involved in transcriptional adaptation, and possibly in a gene-dependent manner. $n = 3$ (**a**) or $n = 2$ (**b**, **c**) biologically independent samples. Data are mean ± s.d., and a two-tailed Student's *t*-test was used to calculate *P* values.

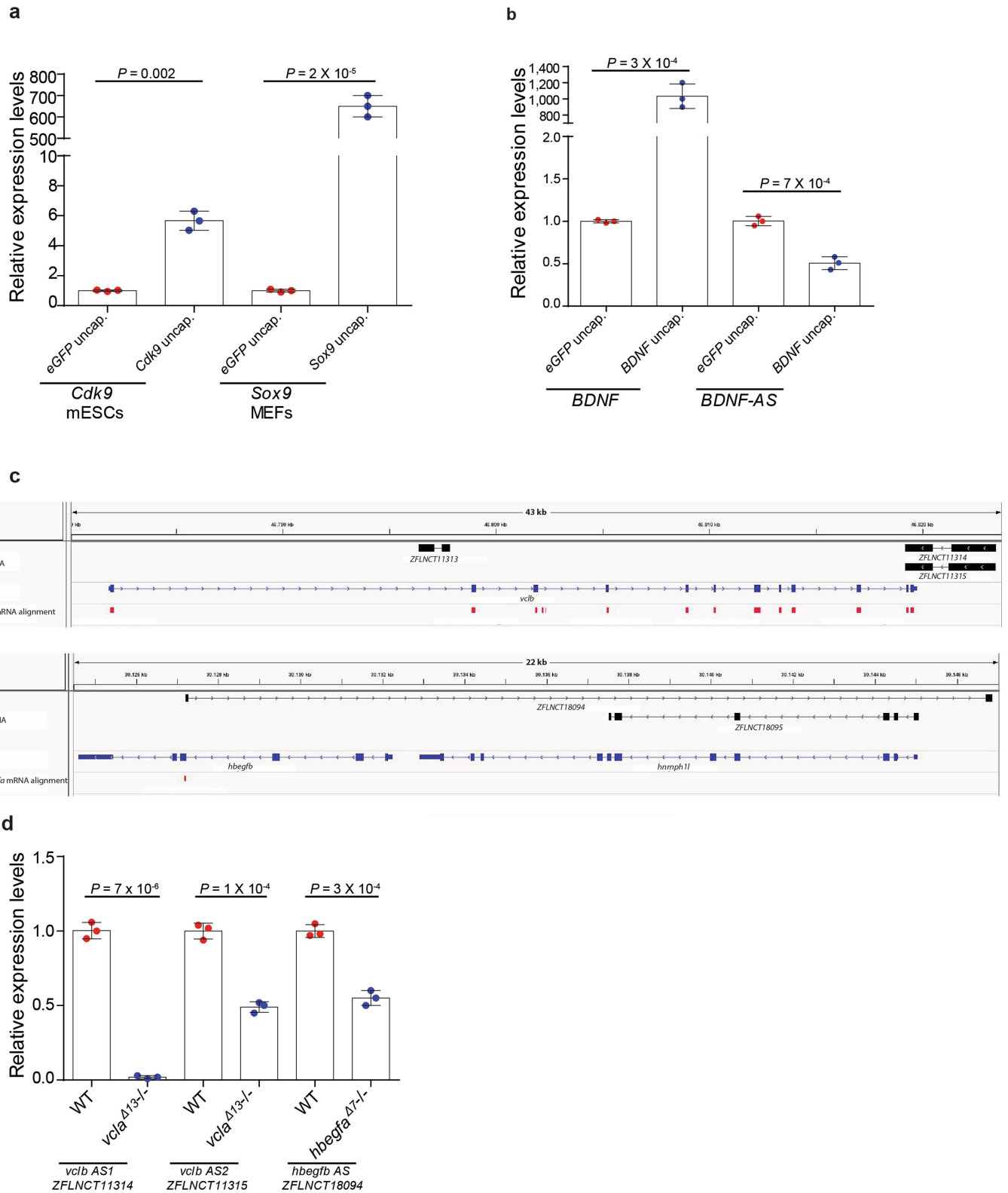

Extended Data Fig. 10 | The potential role of antisense transcripts in the transcriptional adaptation response. a, qPCR analysis of *Cdk9* and *Sox9* mRNA expression levels in cells transfected with uncapped *Cdk9* or *Sox9* RNA. **b**, qPCR analysis of *BDNF* and *BDNF-AS* mRNA expression levels in HEK293T cells transfected with uncapped *BDNF* RNA. **c**, Integrated genome viewer tracks of *vclb* and *hbegfb* loci, showing the location of the annotated antisense transcripts. Two alignments of 105 and 147 bp were observed between *vcla* mRNA and *vclb* antisense RNAs, and an alignment of 39 bp was observed between *hbegfa* mRNA and *hbegfb* antisense RNA. Antisense transcripts shown were acquired from the datasets in GSE32898. **d**, qPCR analysis of *vclb* and *hbegfb* antisense (AS) RNA expression levels in *vcla* and *hbegfa* wild-type and mutant zebrafish at 24 and 72 hpf, respectively. Control expression levels were set at 1 for each assay. $n = 3$ biologically independent samples. Data are mean ± s.d., and a two-tailed Student's *t*-test was used to calculate *P* values.

nature research

Corresponding author(s): Didier Stainier

Last updated by author(s): Jan 11, 2019

Reporting Summary

Nature Research wishes to improve the reproducibility of the work that we publish. This form provides structure for consistency and transparency in reporting. For further information on Nature Research policies, see Authors & Referees and the Editorial Policy Checklist.

Statistics

For all statistical analyses, confirm that the following items are present in the figure legend, table legend, main text, or Methods section.

n/a	Confirmed	
☐	☒	The exact sample size (*n*) for each experimental group/condition, given as a discrete number and unit of measurement
☐	☒	A statement on whether measurements were taken from distinct samples or whether the same sample was measured repeatedly
☐	☒	The statistical test(s) used AND whether they are one- or two-sided *Only common tests should be described solely by name; describe more complex techniques in the Methods section.*
☐	☒	A description of all covariates tested
☐	☒	A description of any assumptions or corrections, such as tests of normality and adjustment for multiple comparisons
☐	☒	A full description of the statistical parameters including central tendency (e.g. means) or other basic estimates (e.g. regression coefficient) AND variation (e.g. standard deviation) or associated estimates of uncertainty (e.g. confidence intervals)
☐	☒	For null hypothesis testing, the test statistic (e.g. *F*, *t*, *r*) with confidence intervals, effect sizes, degrees of freedom and *P* value noted *Give P values as exact values whenever suitable.*
☒	☐	For Bayesian analysis, information on the choice of priors and Markov chain Monte Carlo settings
☒	☐	For hierarchical and complex designs, identification of the appropriate level for tests and full reporting of outcomes
☒	☐	Estimates of effect sizes (e.g. Cohen's *d*, Pearson's *r*), indicating how they were calculated

Our web collection on statistics for biologists contains articles on many of the points above.

Software and code

Policy information about availability of computer code

Data collection	No Software was used.
Data analysis	No Software was used.

For manuscripts utilizing custom algorithms or software that are central to the research but not yet described in published literature, software must be made available to editors/reviewers. We strongly encourage code deposition in a community repository (e.g. GitHub). See the Nature Research guidelines for submitting code & software for further information.

Data

Policy information about availability of data

All manuscripts must include a data availability statement. This statement should provide the following information, where applicable:

- Accession codes, unique identifiers, or web links for publicly available datasets
- A list of figures that have associated raw data
- A description of any restrictions on data availability

ATACseq and RNAseq data were deposited to Gene Expression Omnibus under accession codes GSE107075 and GSE114212.

Field-specific reporting

Please select the one below that is the best fit for your research. If you are not sure, read the appropriate sections before making your selection.

☒ Life sciences ☐ Behavioural & social sciences ☐ Ecological, evolutionary & environmental sciences

For a reference copy of the document with all sections, see nature.com/documents/nr-reporting-summary-flat.pdf

Life sciences study design

All studies must disclose on these points even when the disclosure is negative.

Sample size	No statistical methods were used to predetermine sample size. Sample size was determined according to the minimal number of independent biological replicates that significantly identified an effect. For most qPCR analyses we analyzed 3 sets of biological samples (ie, zebrafish or cultured cells). The variability between the three biological replicates was very minimal and therefore did not require increasing the sample size.
Data exclusions	No data were excluded.
Replication	Experiments in this study were independently replicated, with biological and technical replicates. All attempts at replication were successful, verifying the reproducibility of the findings.
Randomization	The experiments were not randomized due to the required experimental set up (ie, in most experiments, we first had to genotype the zebrafish in order to pool samples).
Blinding	The investigators were not blinded to allocation during experiments and outcome assessment for the reasons mentioned above.

Reporting for specific materials, systems and methods

We require information from authors about some types of materials, experimental systems and methods used in many studies. Here, indicate whether each material, system or method listed is relevant to your study. If you are not sure if a list item applies to your research, read the appropriate section before selecting a response.

Materials & experimental systems

n/a	Involved in the study
☐	☒ Antibodies
☐	☒ Eukaryotic cell lines
☒	☐ Palaeontology
☐	☒ Animals and other organisms
☒	☐ Human research participants
☒	☐ Clinical data

Methods

n/a	Involved in the study
☒	☐ ChIP-seq
☒	☐ Flow cytometry
☒	☐ MRI-based neuroimaging

Antibodies

Antibodies used	The following antibodies were used: KINDLIN-2 (Millipore, MAB2617; clone 3A3, 1:1,000, Lot. 2739149), RELA (Cell Signalling Technology, #6956, 1:1,000), β-ACTIN (Cell Signalling Technology, #8457, 1:1,000), anti-mouse IgG-HRP (Thermo, 31430, 1:10,000, Lot. SG253594), anti-rabbit IgG-HRP (Thermo, 31460, 1:10,000, Lot. TG266717), rabbit IgG (4µg/IP, # 026102, Thermo Fischer, Lot.: TD268143), WDR5 (4µg/IP, #13105, Cell signaling) and H3K4me3 (4µg/IP, #9751, Cell signaling, Lot. 10).
Validation	All antibodies were obtained from the indicated commercial vendors and have been validated for the application by the manufacturer to ensure quality. β-ACTIN, KINDLIN-2 and RELA antibodies were also validated by the authors in the sense that they do not recognize any protein in β-Actin, Kindlin-2 and Rela knockout mouse cells, respectively. Previous ChIP-seq data in mouse cells using the H3K4me3 antibody revealed enrichment at promoter regions (Sodersten et al. PLOS Genetics, 2014). In addition, all the antibodies detected intended proteins in control samples with the expected molecular weight. Specific references for each antibody can be found on the suppliers' homepage.

Eukaryotic cell lines

Policy information about cell lines

Cell line source(s)	mESCs from the C57BL/6 mouse strain were a generous gift from Johnny Kim, MPI for heart and lung research, Bad Nauheim, Germany. Wild-type and Rela knockout MEFs were a generous gift from Alexander Hoffmann, UCLA, USA. Wild-type and Kindlin-2 knockout MKFs were a generous gift from Reinhard Fässler, MPI for biochemistry, Martinsried, Germany.
Authentication	None of the cell lines were authenticated by the authors.
Mycoplasma contamination	All cell lines tested negative for mycoplasma contamination.
Commonly misidentified lines (See ICLAC register)	No commonly misidentified cell lines were used.

Animals and other organisms

Policy information about studies involving animals; ARRIVE guidelines recommended for reporting animal research

Laboratory animals	Zebrafish (Danio rerio), strain: Tüb/AB. All experiments were performed on zebrafish embryos or larvae between 6 hpf and 6 dpf before sex is specified.
Wild animals	The study did not involve wild animals.
Field-collected samples	The study did not involve samples collected from the field.
Ethics oversight	All zebrafish husbandry was performed under standard conditions in accordance with institutional (Max Planck Gesellschaft) and national ethical and animal welfare guidelines approved by the ethics committee for animal experiments at the Regierungspräsidium Darmstadt, Germany (permit number: B2/1017).

Note that full information on the approval of the study protocol must also be provided in the manuscript.